ARTICLE

Vincristine-induced peripheral neuropathy is driven by canonical NLRP3 activation and IL-1β release

Hana Starobova[1], Mercedes Monteleone[1], Christelle Adolphe[1], Lena Batoon[2,3], Cheyenne J. Sandrock[2,3], Bryan Tay[1], Jennifer R. Deuis[1], Alexandra V. Smith[1], Alexander Mueller[1], Evelyn Israel Nadar[1], Grace Pamo Lawrence[1], Amanda Mayor[1], Elissa Tolson[1], Jean-Pierre Levesque[2,3], Allison R. Pettit[2,3], Brandon J. Wainwright[1], Kate Schroder[1], and Irina Vetter[1,4]

Vincristine is an important component of many regimens used for pediatric and adult malignancies, but it causes a dose-limiting sensorimotor neuropathy for which there is no effective treatment. This study aimed to delineate the neuro-inflammatory mechanisms contributing to the development of mechanical allodynia and gait disturbances in a murine model of vincristine-induced neuropathy, as well as to identify novel treatment approaches. Here, we show that vincristine-induced peripheral neuropathy is driven by activation of the NLRP3 inflammasome and subsequent release of interleukin-1β from macrophages, with mechanical allodynia and gait disturbances significantly reduced in knockout mice lacking NLRP3 signaling pathway components, or after treatment with the NLRP3 inhibitor MCC950. Moreover, treatment with the IL-1 receptor antagonist anakinra prevented the development of vincristine-induced neuropathy without adversely affecting chemotherapy efficacy or tumor progression in patient-derived medulloblastoma xenograph models. These results detail the neuro-inflammatory mechanisms leading to vincristine-induced peripheral neuropathy and suggest that repurposing anakinra may be an effective co-treatment strategy to prevent vincristine-induced peripheral neuropathy.

Introduction

Vincristine is a vinca alkaloid used predominantly for the treatment of childhood leukemias and brain cancers, as well as for treatment of several adult tumors. The main side effect of vincristine is a peripheral neuropathy characterized by motoric, autonomic, and sensory symptoms, such as gait abnormalities, obstipation, 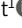or changes in the perception of mechanical or vibration stimuli (Mora et al., 2016; Starobova and Vetter, 2017). Vincristine-induced peripheral neuropathy (VIPN) is thus a serious dose-limiting side effect contributing to morbidity and reduced quality of life in patients treated with vincristine (Kautio et al., 2011; Nama et al., 2020).

The exact pathophysiological mechanisms underlying VIPN remain unclear, which has hampered the development of effective treatment strategies that could either prevent or control the symptoms of VIPN. Although vincristine targets microtubules, and impaired retrograde and anterograde transport has been suggested as one mechanism leading to altered sensory neuron function, there is growing evidence that chemotherapy-induced neuropathy caused by a diverse range of agents incorporates significant neuro-inflammatory components (Montague et al., 2018; Old et al., 2014; Starobova et al., 2019b). Vincristine, in

particular, induces a striking upregulation of inflammatory genes in dorsal root ganglia (DRG), and release of pro-inflammatory cytokines and chemokines, including IL-1β, TNFα, IL-6, and CCL2, is implicated in the development of VIPN (Kiguchi et al., 2009; Starobova et al., 2019b). Indeed, a causative contribution of infiltrating peripheral macrophages was confirmed in CX_3CR_1- and CCR_2-deficient mice, which develop less mechanical allodynia after treatment with vincristine (Montague et al., 2018; Old et al., 2014). However, the signaling pathways leading to cytokine release from these infiltrating peripheral macrophages, as well as the contributions of these mechanisms to the development of vincristine-induced mechanical allodynia, are unknown.

One inflammatory pathway in macrophages involves the activation of the NLRP3 (nucleotide oligomerization domain-like receptor pyrin domain–containing 3) inflammasome, which leads to the release of pro-inflammatory cytokines, such as IL-1β and IL-18. We thus sought to elucidate the contribution of the NLRP3 inflammasome and resultant cytokine release to VIPN.

Here, we demonstrate that vincristine elicits release of IL-1β from human and murine macrophages via a caspase-1–dependent,

[1]Institute for Molecular Bioscience, The University of Queensland, St. Lucia, Queensland, Australia; [2]Mater Research Institute and Faculty of Medicine, The University of Queensland, Woolloongabba, Queensland, Australia; [3]Translational Research Institute, Woolloongabba, Queensland, Australia; [4]The School of Pharmacy, The University of Queensland, Woolloongabba, Queensland, Australia.

Correspondence to Irina Vetter: i.vetter@uq.edu.au; Kate Schroder: k.schroder@imb.uq.edu.au.
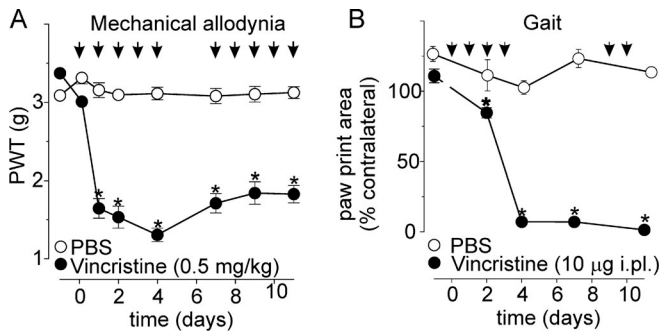
Figure 1. **A murine model of vincristine-induced neuropathy recapitulates sensory and gait abnormalities. (A)** Vincristine (black circles; $n = 6$) causes a decrease of mechanical PWTs in C57BL/6J mice compared with PBS-treated animals (white circles; $n = 6$). **(B)** Vincristine (black circles; $n = 6$) causes gait abnormalities, evidenced by a decrease of paw print area (cm²) relative to the contralateral control (PBS, white circles). Black arrows in A and B indicate the time points of vincristine administration. Statistical significance was determined by repeated measures two-way ANOVA with Sidak's multiple comparisons test; data are shown as mean ± SEM. *, P < 0.05.

canonical NLRP3 signaling pathway, and that VIPN fails to develop in IL-1 receptor (IL1R)– and IL-1β–deficient mice. Importantly, the clinically used IL1R antagonist anakinra prevented development of vincristine-induced gait abnormalities and mechanical allodynia without affecting the chemotherapy efficacy of vincristine—or tumor growth—in medulloblastoma patient-derived xenograft (PDX) models. These results suggest that treatment with anakinra may be a viable clinical strategy to prevent development of VIPN without adversely affecting cancer treatment outcomes.

Results

Peripheral neuro-inflammation causes vincristine-induced mechanical allodynia

Patients treated with vincristine develop sensory disturbances, such as hyperesthesia or altered responses to light touch and pinprick, as well as motoric disturbances, including altered gait and foot drop syndrome (Kautio et al., 2011). These symptoms are recapitulated in murine models based on i.p. or intraplantar (i.pl.) administration of vincristine (Old et al., 2014; Starobova et al., 2019a; Uçeyler et al., 2006). Specifically, as previously described, systemic and local treatment with vincristine (0.5 mg/kg i.p., 10 doses/12 d; or 10 µg i.pl., 6 doses/12 d) elicited pronounced mechanical allodynia as evidenced by a significant decrease in mechanical paw withdrawal thresholds (PWTs; Fig. 1 A and Table S1). In addition to mechanical allodynia, gait abnormalities were also apparent in animals treated with vincristine (10 µg i.pl.; Fig. 1 B and Table S1); however, vincristine did not induce changes in weight gain, general well being, gross motor performance, or heat PWTs (Fig. S1).

In light of recent evidence suggesting a significant neuroinflammatory component of VIPN (Montague et al., 2018; Old et al., 2014; Starobova et al., 2019a) and observations that the longest axons are affected first (Wang et al., 2000), we sought to confirm the previously reported (Old et al., 2014) vincristine-induced infiltration of F4/80+ (pan-macrophage marker) cells

into the sciatic nerve, which harbors some of the longest sensory axons innervating the plantar hind paw. In the sciatic nerve of PBS-treated C57BL/6J mice, we observed a small number of F4/80+ cells consistent with levels expected in healthy tissue (94.5 ± 12.2 cells/ mm²; $n = 7$; Fig. 2, A and C). In contrast, treatment with vincristine (0.5 mg/kg i.p., 24 h) caused increased infiltration of F4/80+ cells into the sciatic nerve (141.4 ± 16.4 cells/ mm²; $n = 7$; Fig. 2, B and C; P < 0.05 compared with PBS control). In addition, treatment with vincristine caused a significant (P < 0.05 compared with PBS control) increase in the number of F4/80+ cells in DRG (Fig. 2, D–F; PBS control: 299.6 ± 46.2 cells/mm²; vincristine: 619.2 ± 58.3 cells/mm²), but not in the spinal cord (Fig. 2, G–I; PBS control: 7.5 ± 0.4 cells/mm²; vincristine: 11.7 ± 1.7 cells/mm²).

To confirm that infiltrating immune cells contribute to VIPN, we next assessed vincristine-induced mechanical allodynia in immune cell–depleted animals. Granulocytes were depleted using an anti-Ly6G antibody, and macrophages were depleted using clodronate liposomes before administration of vincristine. Compared with control, treatment with liposomal clodronate significantly (P < 0.05) reduced the number of F4/80+ cells in spleen (Fig. 2, J–L; PBS control: 6.73 ± 1.57%; liposomal clodronate: 2.94 ± 1.24%) and also reversed the number of F4/80+ cells in the sciatic nerve of vincristine-treated animals to baseline levels (Fig. 2 M). Similarly, treatment with anti-Ly6G antibody significantly reduced the proportion of granulocytes in circulating blood from 5.33 ± 0.88% to 1.00 ± 0.00% of total live cell counts as determined by flow cytometry compared with the isotype control antibody (Fig. 2 N).

Consistent with infiltrating F4/80+ cells driving the development of VIPN, macrophage depletion prevented the vincristine-induced decrease of mechanical PWT (Fig. 2 O; vincristine + PBS: 1.62 ± 0.23 g; vincristine + liposomal clodronate: 2.99 ± 0.15 g; P < 0.001). In contrast, granulocyte depletion did not affect vincristine-induced mechanical allodynia, as the mechanical thresholds of animals treated with anti-Ly6G (1.57 ± 0.30 g) were not significantly (P > 0.05) different from those of isotype antibody–treated animals (1.24 ± 0.17 g; Fig. 2 O). Macrophages, and not neutrophils, are thus key cellular drivers of VIPN.

The NLRP3 inflammasome is required for vincristine-induced mechanical allodynia and gait abnormalities

NLRP3 is mainly expressed in myeloid cells, including F4/80+ macrophages, and NLRP3 inflammasome signaling contributes to the inflammatory responses induced by microbial and sterile danger signals. In light of increasing evidence suggesting a crucial contribution of the NLRP3 inflammasome to many diseases involving sterile inflammation (Mangan et al., 2018), we next sought to investigate development of VIPN in *Nlrp3*−/− mice. *Nlrp3* deficiency indeed prevented vincristine-induced mechanical allodynia (Fig. 3 A and Table S2) and gait abnormalities (Fig. 3 B and Table S3).

Notably, we did not observe any phenotypic differences between early and late vincristine-induced neuropathy, with *Nlrp3*−/− mice protected from symptoms over the entire 25-d observation period, suggesting that mechanisms leading to
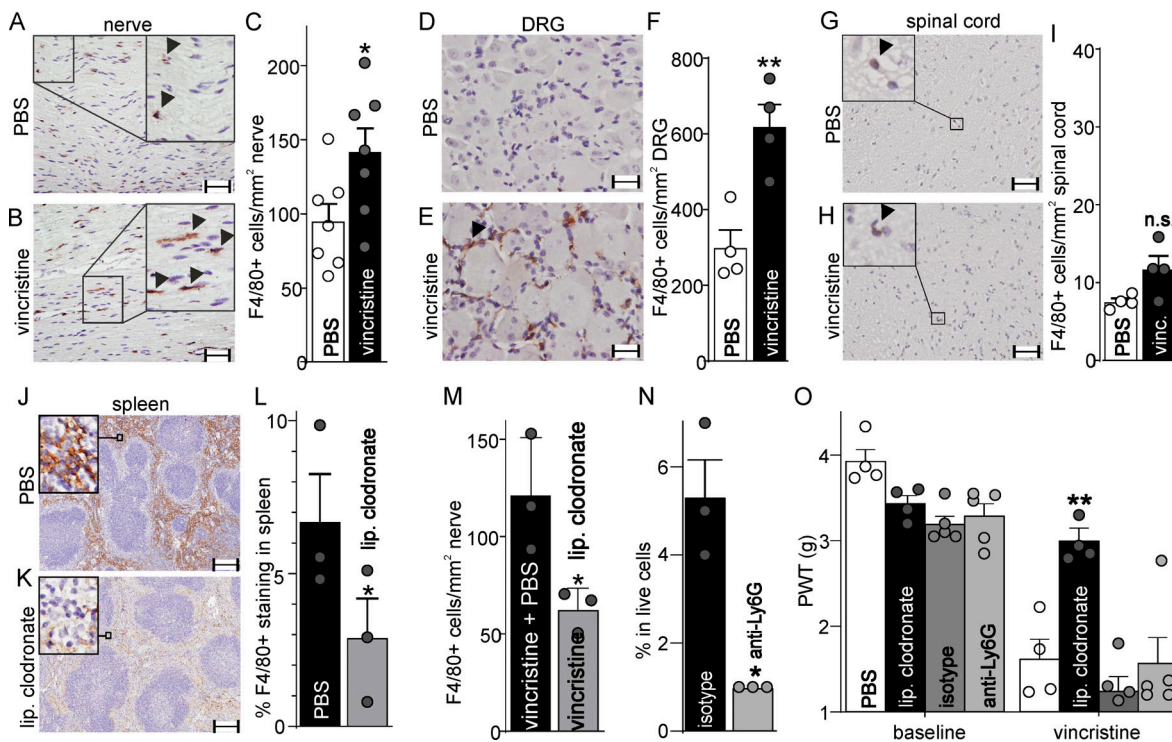
Figure 2. **VIPN is driven by infiltrating macrophages. (A–I)** Vincristine (vinc) causes infiltration of F4/80$^+$ cells (arrows; brown due to diaminobenzidine chromogen) into the sciatic nerve (A–C) and DRGs (D–F), but not spinal cord (G–I). Representative IHC images of sciatic nerve (A and B), DRG (D and E), and spinal cord (G and H) sections from C57BL/6J mice. Scale bar: 50 µm. **(J–L)** Depletion of macrophages by liposomal clodronate was confirmed by quantitative anti-F4/80$^+$ staining of spleen (J and K, representative IHC images; scale bar: 200 µm). The inset in J and K is a magnified view showing F4/80$^+$ cells. **(M)** Compared with PBS-treated animals, treatment with liposomal clodronate (lip. clodronate; 50 µg/g i.p.; 24 h) significantly decreased the number of F4/80$^+$ cells infiltrating the sciatic nerve of animals after vincristine administration. **(N)** Depletion of granulocytes in circulating blood after treatment with anti-Ly6G antibody (200 µg i.p.) compared with the isotype control antibody (200 µg); confirmed by flow cytometry. **(O)** Depletion of macrophages with liposomal clodronate (black bars), but not granulocytes (light gray bars), reverses development of vincristine-induced mechanical allodynia compared with vehicle (white bars) and isotype antibody control (dark gray bars). Statistical significance was determined by unpaired two-tailed t test (C, F, I, L, M, and N) and two-way ANOVA with Tukey's multiple comparisons test (O). Data are shown as mean ± SEM; n = 3–7 for all groups as indicated. *, P < 0.05; **, P < 0.01.

VIPN are not subject to temporal variances observed in *Cx3cr1*-deficient mice (Old et al., 2014). We thus focused our behavioral observations to 11 d after vincristine for subsequent in vivo experiments. In keeping with key pathophysiological function for NLRP3 in VIPN, C57BL6/J mice treated with the selective NLRP3 inhibitor MCC950 (Coll et al., 2019) were protected from both mechanical allodynia (Fig. 3 A and Table S2) and gait abnormalities (Fig. 3 B and Table S3) induced by vincristine.

Vincristine induces IL-1β release from human and murine macrophages

Following exposure to priming signals that lead to transcriptional upregulation of NLRP3, activation of the NLRP3 inflammasome drives the release of IL-1β, a pro-inflammatory cytokine known to sensitize nociceptors (Binshtok et al., 2008). We thus next examined IL-1β release in macrophages treated with vincristine. In LPS-primed human monocyte–derived macrophages, treatment with vincristine (4 h; 100 µM) caused significant release of IL-1β (312.31 ± 169.14 pg/ml) compared with control (11.70 ± 4.56 pg/ml), although this was modest compared with the strong NLRP3 agonist, nigericin (5 µM; 2,759.45 ± 399.35 pg/ml, 45 min; Fig. 3 C). Similarly, vincristine caused a modest but significant release of IL-1β in LPS-primed bone

marrow–derived macrophages (BMMs) from C57BL6/J mice (control: 0 ± 0 pg/ml; vincristine: 231.50 ± 43.71 pg/ml; P < 0.05), but not in unprimed macrophages (control: 0 ± 0 pg/ml; vincristine: 0 ± 0 pg/ml; Fig. 3 D). To better understand the signaling pathways that lead to vincristine-induced IL-1β release, we also investigated the ability of vincristine to independently prime the NLRP3 inflammasome. Interestingly, vincristine-primed BMMs released negligible amounts of IL-1β in response to the NLRP3 activator nigericin (5 µM; 30.42 ± 2.76 pg/ml), while nigericin induced considerable IL-1β release in LPS-primed BMMs (4,749.00 ± 194.50 pg/ml; Fig. 3 E). Similarly, vincristine treatment did not lead to increased expression of NLRP3 in macrophages (Fig. S2 A). Together, these results indicate that vincristine does not prime the NLPR3 inflammasome, but instead functions as a bona fide activation signal for NLRP3 signaling.

To determine whether vincristine-induced IL-1β release could occur as a result of cell death and the subsequent release of danger-associated molecular patterns (DAMPs), we also assessed lactate dehydrogenase (LDH) release in LPS-primed and -unprimed macrophages. However, marked LDH release was not observed under conditions leading to robust IL-1β release (max LDH release [% control]: negative control [+LPS]: 7.164 ± 0.28%;

Starobova et al.
Inhibition of IL-1β release prevents VIPN

Journal of Experimental Medicine   3 of 16
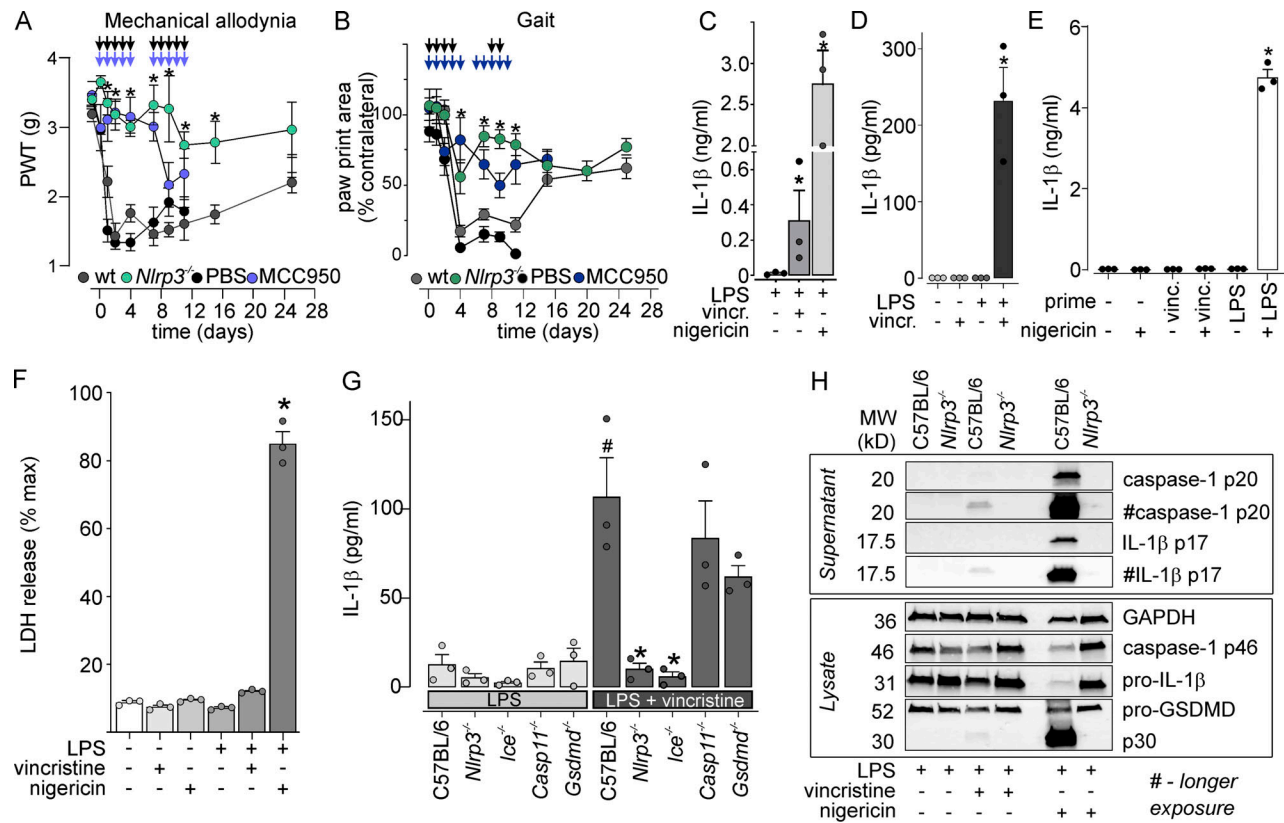https://doi.org/10.1084/jem.20201452

Figure 3. Vincristine leads to activation of the NLRP3-inflammasome and IL-1β release. (A) Mechanical allodynia induced by vincristine (vinc or vincr; 0.5 mg/kg i.p.) does not develop in *Nlrp3*^{−/−} animals (green symbols) and is attenuated by the NLRP3 antagonist MCC950 (blue symbols; 20 mg/kg i.p.) compared with wt (dark gray symbols) and PBS-treated (black symbols) controls, respectively. Black arrows indicate vincristine administration schedule and colored arrows indicate MCC950 treatment schedule. *n* = 6 for all groups. **(B)** The decrease in paw print area induced by vincristine (10 μg i.pl.) is abolished in *Nlrp3*^{−/−} animals (dark green) and after treatment with MCC950 (dark blue; 20 mg/kg i.p.) compared with wt (dark gray symbols) and PBS-treated (black symbols) controls, respectively. Black arrows indicate vincristine administration schedule and colored arrows indicate MCC950 treatment schedule. Statistical significance was determined by using two-way ANOVA with Tukey's multiple comparisons test. All data are shown as mean ± SEM; *n* = 6 for all groups. *, P < 0.05. **(C and D)** Vincristine induces significant release of IL-1β in human (C) and mouse (D) LPS-primed macrophages. **(E)** Incubation of BMMs with vincristine does not prime the NLRP3 inflammasome. Nigericin (5 μM) treatment leads to release of IL-1β in LPS-primed, but not vincristine-primed, macrophages. **(F)** Vincristine treatment does not induce marked cell death, expressed as percentage of LDH release of 100% lysis control. **(G)** Vincristine-induced release of IL-1β is abolished in *Nlrp3*^{−/−} and *Ice*^{−/−}, but not in *Casp11*^{−/−} or *Gsdmd*^{−/−} LPS-primed BMMs. *, P < 0.05 cf. C57BL/6 (LPS); #, P < 0.05 cf. C57BL/6 (LPS + vincristine). **(H)** Cleaved IL-1β (p17) and caspase-1 (p20) are found in supernatants of vincristine-treated C57BL6/J, but not *Nlrp3*^{−/−}, LPS-primed BMMs. (C–G) Statistical significance was determined using one-way ANOVA. All data are shown as mean ± SEM; *n* = 3 for all groups. *, P < 0.05. MW, molecular weight.

vincristine: 12.09 ± 0.28%, positive control [+LPS + nigericin 5 μM]: 85.00 ± 3.58%; Fig. 3 F), suggesting that vincristine-induced NLRP3 signaling is not a result of cell death–induced release of DAMPs and subsequent NLRP3 activation.

The NLRP3 inflammasome signals via caspase-1 to cleave and activate the pyroptotic effector gasdermin-D (GSDMD). NLRP3 can be activated directly via the canonical signaling pathway or indirectly via a noncanonical pathway that requires caspase-11 (for review, see Kelley et al., 2019). We thus next assessed IL-1β release in BMMs derived from wt, *Nlrp3*^{−/−}, *Ice*^{−/−} (*Casp1*^{−/−}/*Casp11*[null/null]; Kayagaki et al., 2011), *Casp11*^{−/−}, or *Gsdmd*^{−/−} animals. In WT BMMs, vincristine induced IL-1β release (106.8 ± 22.2 pg/ml; Fig. 3 G) and cleavage of pro–IL-1β, caspase-1, and GSDMD (Fig. 3 H). Consistent with the crucial contribution of NLRP3 to vincristine-induced gait abnormalities and mechanical allodynia, vincristine-induced IL-1β cleavage and release was abolished in BMMs isolated from *Nlrp3*^{−/−} animals (10.09 ± 3.37 pg/ml; Fig. 3, G and H) and after treatment with the NLRP3

inhibitor MCC950 (1.14 ± 1.14 pg/ml). Indeed, IL-1β release was also decreased in BMMs from *Ice*^{−/−} animals (lacking caspase-1 and caspase-11; control: 2.46 ± 0.75 pg/ml; vincristine: 5.85 ± 2.65 pg/ml), but was not significantly affected by *Casp11* deficiency (control: 10.53 ± 3.52 pg/ml; vincristine: 83.59 ± 21.06) or *Gsdmd* deficiency (control: 14.56 ± 7.29 pg/ml; vincristine: 62.01 ± 6.15; Fig. 3 G). The profile of vincristine-induced IL-1β release is thus reminiscent of canonical NLRP3 activation induced by the prototypical agonist nigericin, which also caused cleavage of pro–IL-1β, caspase-1, and GSDMD (Fig. 3 H), as well as release of mature IL-1β that is dependent on caspase-1, but not caspase-11 (Fig. S2 B).

To further demonstrate that NLRP3 activation in macrophages is a key contributor to vincristine-induced allodynia, we next isolated BMMs from wt and *Nlrp3*^{−/−} animals, and administered cells treated with vincristine in vitro into naive wt animals via local i.pl. injection (Fig. 4 A). Consistent with our results showing IL-1β release in LPS-primed, vincristine-treated
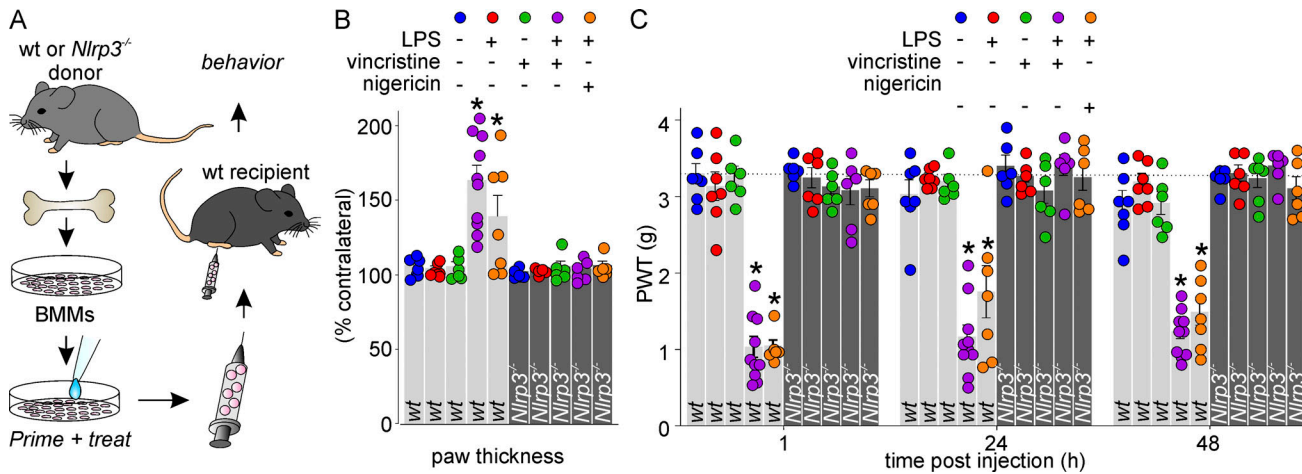
Starobova et al.
Inhibition of IL-1β release prevents VIPN

Journal of Experimental Medicine
https://doi.org/10.1084/jem.20201452

Figure 4. **Intraplantar injection of vincristine-treated macrophages in naive animals causes mechanical allodynia. (A)** Schematic illustrating the experimental design. BMMs isolated from WT or $Nlrp3^{-/-}$ animals were primed and treated in vitro, harvested, and administered to naive animals via i.pl. injection. **(B)** Intraplantar injection of LPS-primed macrophages treated with vincristine (purple) or nigericin (orange), but not untreated (blue), LPS-primed (red), unprimed vincristine-treated (green), or $Nlrp3^{-/-}$ macrophages (dark gray bars) causes unilateral paw swelling. n = 6–10 animals/group. **(C)** Intraplantar injection of LPS-primed macrophages treated with vincristine (purple) or nigericin (orange), but not untreated (blue), LPS-primed (red), or unprimed vincristine-treated (green) cells causes mechanical allodynia. Intraplantar injection of macrophages from $Nlrp3^{-/-}$ animals does not cause mechanical allodynia, irrespective of priming or treatment (dark gray bars). Dotted line indicates baseline PWT. n = 6–10 animals/group. Statistical significance was determined using one-way ANOVA. *, P < 0.05.

macrophages (Fig. 3 C and D), local administration of LPS-primed macrophages treated with vincristine or nigericin elicited mechanical allodynia (PWT: untreated control: 3.3 ± 0.1 g; LPS: 3.1 ± 0.2 g; LPS + vincristine: 1.0 ± 0.1 g; LPS + nigericin: 1.0 ± 0.1 g) and unilateral paw swelling (% contralateral paw thickness: untreated control: 106 ± 2%; LPS: 104 ± 2%; LPS + vincristine: 163 ± 10%; LPS + nigericin: 139 ± 14%) lasting for 48 h (Fig. 4, B and C). In contrast, administration of neither unprimed, vincristine-treated macrophages nor LPS-primed, vincristine-treated $Nlrp3^{-/-}$ macrophages caused paw swelling (% contralateral paw thickness: unprimed + vincristine: 106 ± 3%; LPS + vincristine $Nlrp3^{-/-}$: 106 ± 4%) or mechanical allodynia (PWT: unprimed + vincristine: 3.3 ± 0.1 g; LPS + vincristine $Nlrp3^{-/-}$: 3.1 ± 0.1 g; Fig. 4, B and C).

Canonical NLRP3 signaling pathways contribute to vincristine-induced mechanical allodynia

To further confirm the contribution of the NLRP3 pathway to the development of mechanical hypersensitivity and gait disturbances in vivo, we next investigated changes in PWT and paw print area in $Ice^{-/-}$, $Casp11^{-/-}$, and $Gsdmd^{-/-}$ animals following treatment with vincristine. Indeed, vincristine-induced mechanical allodynia was significantly reduced (P < 0.05, repeated measures two-way ANOVA with Sidak's multiple comparison correction) in $Ice^{-/-}$ and $Gsdmd^{-/-}$ animals, but not in $Casp11^{-/-}$, compared with wt controls (Fig. 5, A–C; Table S4; and Table S5). Specifically, the vincristine-induced decrease in PWT was attenuated in $Ice^{-/-}$ animals for the first 7 d and PWT values were significantly different (P < 0.05) from wt animals (dotted line, cohort control as in Fig. 3 A) on days 1, 2, 4, and 7 (Fig. 5 A). Similarly, mechanical allodynia was attenuated in $Gsdmd^{-/-}$ animals, with PWT values significantly different from cohort controls (Fig. 5 C, Table S4, and Table S5). In $Casp11^{-/-}$ animals,

PWTs were not significantly different from wt controls (Fig. 5 B, Table S4, and Table S5).

To confirm that NLRP3-mediated IL-1β release contributes to the phenotype of vincristine-induced neuropathy, we also quantified mechanical allodynia in $Il1b^{-/-}$ and $Il1r1^{-/-}$ mice lacking IL-1β and IL1R, respectively (Fig. 5, D and E). Strikingly, $Il1b^{-/-}$ animals did not develop mechanical allodynia (P > 0.05; repeated measures two-way ANOVA time factor comparison with Dunnett's multiple comparisons test) and PWTs oscillated around baseline values. Accordingly, PWTs in $Il1b^{-/-}$ animals were significantly (P < 0.05) different at all time points compared with cohort littermate control (Fig. 5 D, Table S6, and Table S7). Similarly, the PWTs of $Il1r1^{-/-}$ animals were significantly (P < 0.05) higher than control at days 1, 2, and 4 (Fig. 5 E, Table S6, and Table S7).

Sensory neurons can detect IL-1β, with this cytokine directly activating and sensitizing nociceptors via modulation of tetrotodoxin-resistant voltage-gated sodium channels (Na$_V$; Amaya et al., 2006; Binshtok et al., 2008). Specifically, $Na_V1.9^{-/-}$ animals display partially reduced mechanical allodynia after i.pl. injection of IL-1β (Amaya et al., 2006), and we thus sought to assess whether vincristine-induced mechanical sensitization also involves Na$_V$1.9. Indeed, consistent with the phenotype observed after direct administration of IL-1β, $Na_V1.9^{-/-}$ animals were partially protected from vincristine-induced mechanical allodynia, with PWTs significantly different from controls on days 1 and 2 of vincristine treatment (Fig. 5 F, Table S6, and Table S7).

NLRP3 signaling contributes to vincristine-induced gait disturbances

To confirm that both mechanical allodynia and gait disturbances induced by vincristine are driven by similar mechanisms, we
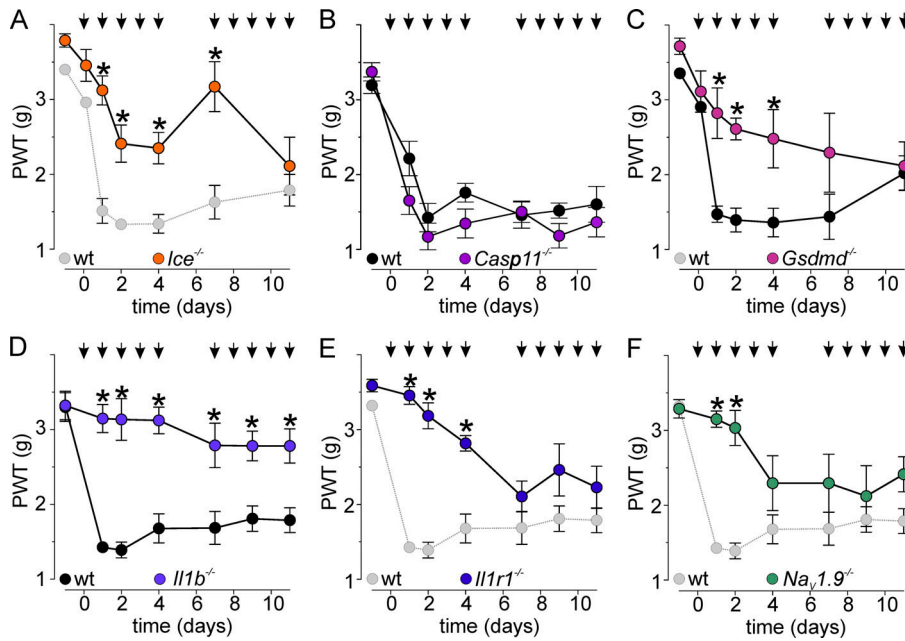
Starobova et al.
Inhibition of IL-1β release prevents VIPN

Journal of Experimental Medicine   5 of 16
https://doi.org/10.1084/jem.20201452

Figure 5. **The canonical NLRP3 signaling pathway contributes to vincristine-induced mechanical allodynia. (A–E)** Mechanical allodynia induced by treatment with vincristine (black arrows; 0.5 mg/kg i.p.) is attenuated in (A) *Ice⁻/⁻* animals (orange symbols; dotted line and light gray symbols are cohort controls also shown in Fig. 3 A); not attenuated in (B) *Casp11⁻/⁻* animals (purple symbols) relative to wt controls (black symbols); attenuated in (C) *Gsdmd⁻/⁻* animals (pink symbols; black symbols are cohort controls); and attenuated in (D) *Il1b⁻/⁻* animals relative to wt controls (black symbols) and (E) *Il1r1⁻/⁻* animals (dotted line and light gray symbols are cohort controls also shown in D). **(F)** In *Na_V1.9⁻/⁻* animals, mechanical allodynia induced by vincristine (0.5 mg/kg; i.p.) is partially attenuated; dotted line and light gray symbols are cohort controls also shown in D. Statistical significance was determined using repeated measures two-way ANOVA with Sidak's multiple comparisons test. All data are shown as mean ± SEM; *n* = 6 for all groups. *, P < 0.05.

next assessed gait disturbances in *Ice⁻/⁻*, *Casp11⁻/⁻*, *Gsdmd⁻/⁻*, *Il1b⁻/⁻*, *Il1r1⁻/⁻*, and *Na_V1.9⁻/⁻* animals. Similar to our findings with vincristine-induced mechanical allodynia, the decrease in paw print area following vincristine treatment (10 µg i.pl.) was partially inhibited in *Ice⁻/⁻* animals and significantly different from cohort controls (dotted line, control data shown in Fig. 3 B) on days 7 and 11 (Fig. 6 A and Table S8).

Consistent with the results shown in Fig. 5 C, vincristine-induced gait abnormalities were also decreased in *Gsdmd⁻/⁻* animals (Fig. 6 C and Table S8). Interestingly, *Casp11⁻/⁻* animals were also partially protected from gait abnormalities (Fig. 6 B and Table S8), implying that motoric symptoms involve additional signaling pathways or cell types. Compared with the

cohort control, paw print area values were significantly different for both *Gsdmd⁻/⁻* and *Casp11⁻/⁻* animals on multiple days (Fig. 6, B and C; and Table S8). Additionally, *Il1b⁻/⁻* animals were protected from development of gait disturbances, with the paw print area of *Il1b⁻/⁻* mice significantly (P < 0.05) increased compared with cohort controls (Fig. 6 D and Table S9). *Il1r1⁻/⁻* mice also only slowly developed a partial gait disturbance (Fig. 6 E and Table S9), with paw print area values significantly different from cohort control (dotted line, control data shown in Fig. 6 D) on days 4 and 7. In contrast, *Na_V1.9⁻/⁻* animals were not protected from vincristine-induced gait disturbances, although there was a nonsignificant trend toward increased paw print areas on days 4 and 7 (Fig. 6 F and Table S9).
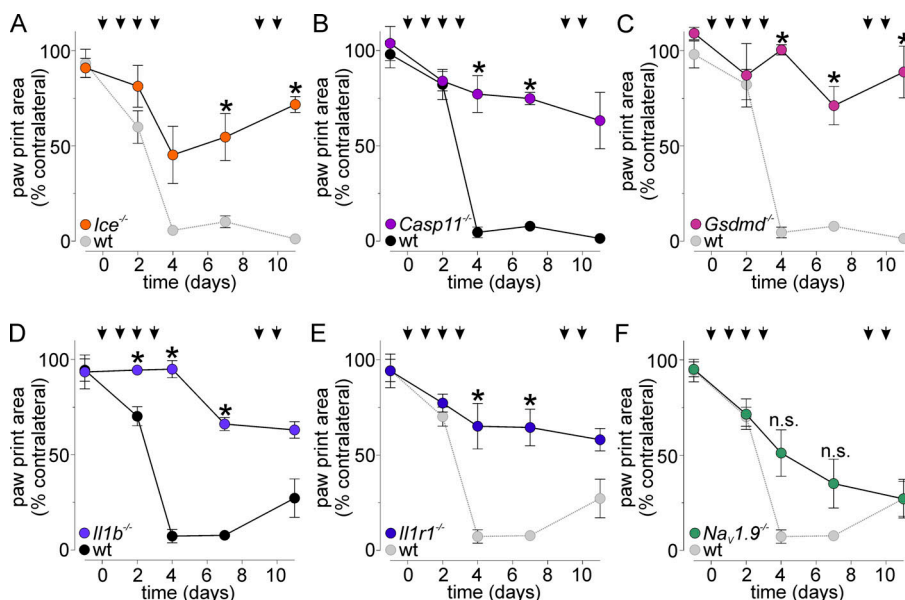
Figure 6. **NLRP3 signaling contributes to vincristine-induced gait disturbances. (A–E)** Gait disturbances, evidenced by a decrease in the ipsilateral paw print area (shown as percentage of contralateral), induced by treatment with vincristine (black arrows; 10 µg i.pl.) are attenuated in (A) *Ice⁻/⁻* animals (orange symbols; dotted line and light gray symbols are cohort controls also shown in Fig. 3 B); (B) *Casp11⁻/⁻* animals (purple symbols) relative to wt controls (black symbols); (C) *Gsdmd⁻/⁻* animals (pink symbols; dotted line and light gray symbols are cohort controls also shown in B); (D) *Il1b⁻/⁻* animals relative to wt controls (black symbols); and (E) *Il1r1⁻/⁻* animals (dotted line and light gray symbols are cohort controls also shown in D). **(F)** In *Na_V1.9⁻/⁻* animals, gait disturbances induced by vincristine are not significantly decreased; dotted line and light gray symbols are cohort controls also shown in D. Statistical significance was determined using repeated measures two-way ANOVA with Sidak's multiple comparisons test. All data are shown as mean ± SEM; *n* = 6 for all groups. *, P < 0.05.
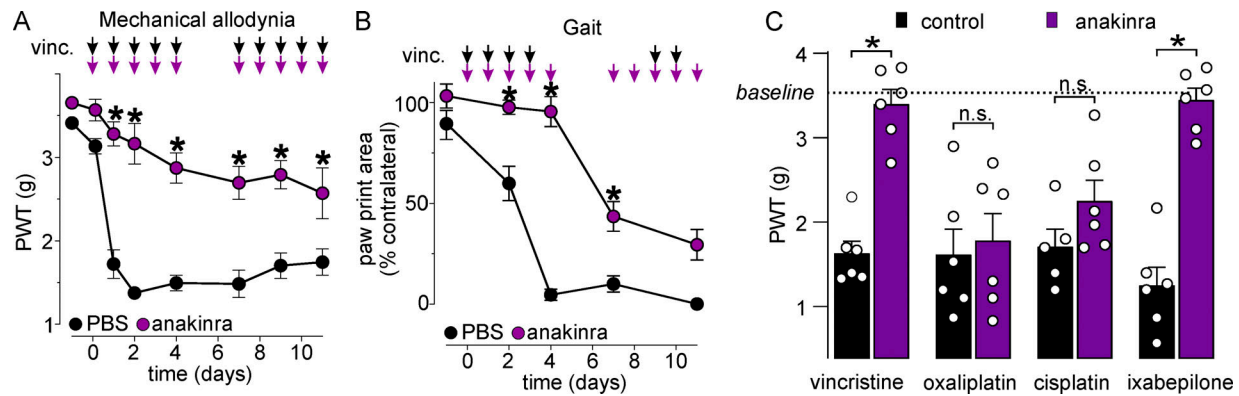
Figure 7. Anakinra treatment prevents the development of VIPN. (A) In animals receiving vincristine (vinc; 0.5 mg/kg i.p.), coadministration of anakinra (purple symbols; 100 mg/kg i.p.) fully prevents development of mechanical allodynia compared with animals treated with vehicle (black symbols; PBS i.p.). $n = 6$ animals/group. **(B)** Gait disturbances induced by vincristine are significantly ($P < 0.05$) delayed in animals treated with anakinra (purple symbols; 100 mg/kg i.p.) compared with animals treated with vehicle (black symbols; PBS i.p.). Black arrows indicate vincristine administration, and purple arrows indicate anakinra/PBS administration schedule. $n = 6$ animals/group. **(C)** Anakinra (100 mg/kg i.p., purple bars) reverses vincristine- and ixabepilone-, but not oxaliplatin- or cisplatin-induced mechanical allodynia. $n = 6$ animals/group. Statistical significance was determined using one-way (C) and repeated measures two-way ANOVA with Sidak's multiple comparisons test (A and B). All data are shown as mean ± SEM. *, $P < 0.05$.

The IL1R antagonist anakinra prevents development of vincristine-induced mechanical allodynia and gait disturbances

NLRP3-mediated diseases, such as familial cold auto-inflammatory syndrome, are currently managed with biologics targeting IL-1β signaling, such as the IL1R antagonist anakinra. We thus sought to evaluate whether anakinra could suppress the development of vincristine-induced mechanical allodynia and gait disturbances. We first confirmed that anakinra doses that have been used in rodent models of acute myocardial infarction, osteosarcoma, and streptozotocin-induced diabetes (Abbate et al., 2008; Baamonde et al., 2007; Vallejo et al., 2014) can effectively prevent IL-1β–mediated pain in a murine model. As previously reported, i.pl. administration of IL-1β in naive animals elicited mechanical allodynia (PWT: baseline: 3.4 ± 0.2 g i.pl.; IL-1β: 1.0 ± 0.1; $P < 0.05$), which was reversed by treatment with anakinra (100 mg/kg i.p.; PWT: 2.8 ± 0.2 g; $P < 0.05$; Fig. S2 C). We next coadministered anakinra (100 mg/kg i.p.) with vincristine (0.5 mg/kg i.p. or 10 μg i.pl.). Anakinra significantly decreased mechanical hypersensitivity (Fig. 7 A and Table S10), with significantly higher PWT values in the anakinra-treated group relative to the vehicle-treated group at all time points. Similarly, the development of gait abnormalities was delayed by treatment with anakinra (100 mg/kg i.p) and was significantly different from vehicle controls (PBS; i.p.; Fig. 7 B and Table S10).

Diverse signaling mechanisms underlie the pathobiology of different types of neuropathic pain, including chemotherapy-induced neuropathy caused by other agents. We thus sought to confirm the effect of anakinra on mechanical allodynia induced by the chemotherapeutics oxaliplatin, cisplatin, and ixabepilone, and observed that coadministration with anakinra (100 mg/kg i.p.) only reversed vincristine- and ixabepilone-, but not oxaliplatin- or cisplatin-induced symptoms (Fig. 7 C), suggesting that the above-described NLRP3 signaling mechanisms may be particularly important in neuropathy induced by tubulin-targeting chemotherapeutics.

To determine the effects of vincristine and anakinra on the function of peripheral nerve terminals, we also performed single-fiber recordings from the murine skin-saphenous nerve preparation. Interestingly, the predominant phenotype elicited by administration of vincristine was a loss of functional myelinated A fibers in the skin-nerve preparation (Fig. S3 A), although intraepidermal nerve fiber density, determined by PGP9.5 immunofluorescence, remained unaffected (Fig. S3, B and C). Crucially, treatment with anakinra prevented this phenotype (Fig. S3 A), confirming previous observations that vincristine-induced functional changes can occur independently of nerve degeneration (Chen et al., 2020).

Treatment with anakinra does not adversely affect tumor progression or vincristine efficacy in medulloblastoma PDX models

The above data demonstrate that NLRP3-dependent IL-1β signaling mediates the symptoms of VIPN, including mechanical allodynia and gait disturbances, and that the IL1R antagonist anakinra can prevent these adverse effects. However, a key consideration of putative antiallodynic treatments is their effect on tumor progression and chemotherapy efficacy. As vincristine is commonly used for the treatment of childhood medulloblastomas, we thus sought to investigate the effect of anakinra in medulloblastoma PDX models. We first confirmed that nigericin- and vincristine-induced IL-1β release was conserved in macrophages from NSG (NOD scid γ) mice (Fig. S4). We then examined this pathway in vivo, with the detailed drug injection schedule shown in Fig. 8 A. Anakinra (100 mg/kg i.p.) indeed protected tumor-bearing NSG mice from developing vincristine-induced allodynia, with anakinra reversing the vincristine-induced decrease in PWTs to values indistinguishable from healthy controls (PWT control: 3.5 ± 0.2 g; PWT anakinra: 3.4 ± 0.2 g; PWT vincristine: 1.1 ± 0.2 g; PWT vincristine + anakinra: 3.2 ± 0.5 g; Fig. 8 B).

For tumor growth in these animals, no significant difference was observed between the groups treated with saline (i.p.) or anakinra (i.p., 100 mg/kg) in the number of days required for
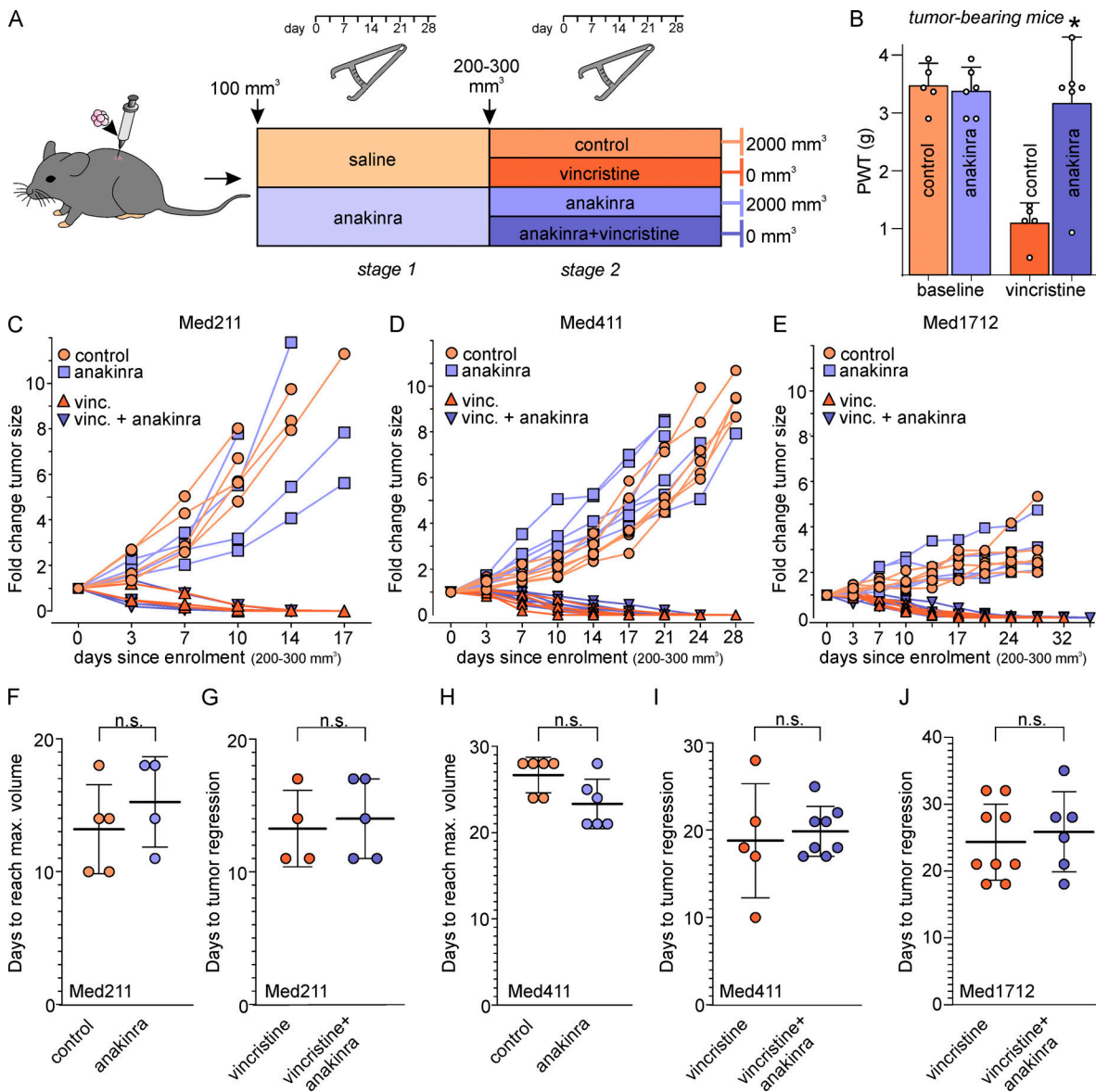
Figure 8. **Anakinra treatment does not affect tumor progression or chemotherapy efficacy. (A)** Detailed time schedule of drug administration in Med-211FH, Med-411FH, and Med-1712FH medulloblastoma PDX models. Mice were injected with Med-211FH, Med-411FH, and Med-1712FH medulloblastoma cells and tumor volume measurements were taken biweekly. Anakinra (light purple) or saline (light orange) treatment commenced when s.c. tumors reached 100 mm³ in size (stage 1). Vincristine (dark orange), anakinra (light purple), saline (light orange), or anakinra + vincristine (dark purple) injections commenced when s.c. tumors reached 300 mm³ in size (stage 2) and treatment was administered for 4 wk daily or until maximum tumor size was reached (2,000 mm³). **(B)** Anakinra (100 mg/kg i.p., purple bars) reverses vincristine-induced mechanical allodynia in tumor-bearing NSG mice. **(C–J)** Effect of anakinra on tumor growth and vincristine-induced complete tumor regression in Med-211FH, Med-411FH, and Med-1712FH medulloblastoma PDX models. **(C–F and H)** Daily treatment with anakinra (light purple) had no effect on time to reach maximum tumor size (2,000 mm³) or tumor growth in animals with an s.c. implanted Med-211FH or Med-411FH tumor compared with controls (light orange symbols). There was also no effect on tumor growth in animals bearing Med-1712FH tumors. **(C–E)** Effect of anakinra on vincristine-induced complete tumor regression in Med-211FH, Med-411FH, and Med-1712FH medulloblastoma PDX models. **(C, D, E, G, I, and J)** Daily treatment with anakinra (dark purple symbols) had no effect on the ability of vincristine to induce regression of Med-211FH (G), Med-411FH (I), or Med-1712FH (J) tumors compared with control animals treated only with vincristine (dark orange symbols). All data are shown as mean ± SEM; $n \geq 4$ animals/group as indicated. *, $P < 0.05$.

Med-211FH and Med-411FH tumors to reach maximum tumor size (2,000 mm³; days to reach maximum volume: Med-211FH saline: 13.0 ± 1.9 d; Med-211FH anakinra: 15.3 ± 1.7 d; Med-411FH saline: 26.6 ± 0.9 d; Med-411FH anakinra: 23.3 ± 1.3 d; Fig. 8, C, F, D, and H). Similarly, the slowly growing Med-1712FH tumors progressed at rates indistinguishable from control during prolonged (28 d) anakinra administration (Fig. 8 E). While tumors

in Med-211FH and Med-411FH tumor-bearing animals that were treated either with vehicle only or anakinra reached maximum tumor size (2,000 mm³) within 10–28 d (Fig. 8, F and H), tumor volume rapidly decreased in all animals receiving vincristine (Fig. 8, C–E and G–J). Specifically, all animals in the Med-211FH group showed complete tumor regression (0 mm³) within 11–17 d of vincristine treatment, while Med-411FH and Med-1712FH tumors

completely regressed within 21–28 and 18–35 d of vincristine treatment, respectively (Fig. 8, G, I, and J).

Importantly, treatment with anakinra did not affect the ability of vincristine to induce complete tumor regression, with quantitative analysis of mice that were cotreated with anakinra and vincristine revealing no significant difference in the number of days for vincristine to induce complete tumor regression (days to tumor regression: Med-211FH vincristine: 13.3 ± 1.4 d; Med-211FH vincristine + anakinra: 14.0 ± 1.3 d; Med-411FH vincristine: 18.8 ± 2.9 d; Med-411FH vincristine + anakinra: 19.8 ± 1.0 d; Med-1712FH vincristine: 24.3 ± 1.9 d; Med-1712FH vincristine + anakinra: 25.8 ± 2.4 d; Fig. 8, G, I, and J). Overall, these results demonstrate that anakinra reduces vincristine-induced neuropathy without adversely affecting cancer progression or chemotherapy efficacy, and indicate that anakinra may be an attractive analgesic cotherapy to vincristine chemotherapeutic regimens.

Discussion

The vinca alkaloids are typically considered cytotoxic anticancer drugs that act during cellular mitosis due to their effects on microtubules. These effects have also been postulated to contribute to neurotoxicity due to effects on the anterograde transport of neuronal proteins (LaPointe et al., 2013). However, in recent years, it has become increasingly clear that vincristine-induced neuropathy is not simply a cell type–specific consequence of the known pharmacological activity of vincristine, but a complex symptom involving considerable neuro-inflammatory components. Specifically, vincristine was shown to induce infiltration of circulating monocytes into peripheral nerves, with CX_3CR_1-positive cells contributing to initiation and CCR_2-positive cells contributing to maintenance of vincristine-induced neuropathy (Montague et al., 2018; Old et al., 2014). Similarly, vincristine treatment leads to a striking upregulation of genes related to immune cell recruitment and inflammatory processes in DRG, consistent with a functional contribution of infiltrating immune cells to vincristine-induced neuronal dysfunction (Starobova et al., 2019b); however, the molecular signaling pathways underpinning these processes have remained elusive. As a major molecular complex mediating macrophage-induced inflammation, we thus investigated whether the NLRP3 inflammasome drives vincristine-induced neuropathy.

NLRP3 is an innate immune sensor for microbial infections and host-derived DAMPs that signal cell damage or stress under sterile inflammatory conditions (Lu et al., 2020). Activation of NLRP3 and its signaling adaptor (ASC) leads to recruitment of the cysteine protease caspase-1, forming a complex termed the inflammasome (Lu et al., 2020). This unleashes caspase-1 protease activity, which, in turn, cleaves and activates the pro-inflammatory cytokines IL-1β and IL-18, as well as the cell executioner GSDMD (Evavold et al., 2018; Mulvihill et al., 2018). Collectively, these so-called canonical NLRP3 signaling processes result in secretion of pro-inflammatory cytokines (Chan and Schroder, 2020).

Release of cytokines after treatment with vincristine has been reported clinically as well as in a range of animal models (Weintraub et al., 1996). Notably, our results show for the first time that vincristine directly causes NLRP3-dependent IL-1β release, paralleled by cleavage of pro-GSDMD and caspase-1, in mouse macrophages. Although IL-1β release was modest compared with the strong NLRP3 activator nigericin, this is perhaps not surprising given that vincristine causes predominantly symptoms of peripheral neuropathy, but not systemic inflammation, such as fever, which is apparent in sepsis or NLRP3-mediated conditions, such as cryopyrin-associated periodic syndrome (Chan and Schroder, 2020). Nonetheless, vincristine-induced allodynia and gait disturbances were significantly reduced in $Nlrp3^{-/-}$, $Ice^{-/-}$, $Gsdmd^{-/-}$, $Il1b^{-/-}$, and $Il1r1^{-/-}$ mice (Fig. 3, Fig. 5, and Fig. 6), suggesting that inflammasome activation and cytokine release likely occurs in immune cells in close proximity to sensory neurons and that these processes are crucial for development of neuropathy. Indeed, we also observed a number of IL-1β–positive cells in the DRG of vincristine-treated animals, although it is not possible to distinguish pro–IL-1β from full-length processed and secreted mature IL-1β using antibodies (Fig. S3). While macrophages infiltrating DRG can certainly contribute to neuropathic pain (Yu et al., 2020), our data suggest that macrophages interacting with peripheral nerves may be sufficient to initiate the development of pain. However, additional studies are required to determine the relative contribution of DRG- and nerve-located macrophages to vincristine-induced neuropathy.

Inflammasome activation typically requires a priming signal, such as ligands for Toll-like receptors or cytokine receptors, that first increase expression of NLRP3 and pro–IL-1β via NF-κB signaling. Interestingly, vincristine-induced IL-1β release was only apparent in primed macrophages, but vincristine was unable to prime the inflammasome, with no IL-1β release apparent in macrophages cotreated with vincristine and nigericin (Fig. 3). The mechanisms leading to vincristine-mediated NLRP3 activation thus seem to differ from the microtubule-stabilizing chemotherapeutic paclitaxel, which does not cause IL-1β release in LPS-primed macrophages, but can directly prime macrophages, leading to activation of caspase-1 by inflammasome-activating signals such as nigericin or ATP (Son et al., 2019). These results are consistent with our previous observation that vincristine-induced neuropathy is reduced in $Tlr4^{-/-}$ mice (Starobova et al., 2019a), although the endogenous signals leading to macrophage priming and NLRP3 activation in vivo in response to vincristine treatment remain unclear. Interestingly, paclitaxel-induced neuropathy was also reversed by anakinra treatment in rats (Kuyrukluyildiz et al., 2016), as was ixabepilone-induced neuropathy in this study (Fig. 7 C), suggesting that NLRP3-driven pathological mechanisms are particularly important for microtubule-targeting agents.

In addition to IL-1β, activation of the NLRP3 inflammasome can also lead to maturation and release of IL-18, which may contribute to the development of pain via activity at the IL-18 receptor (Pilat et al., 2016). Indeed, while we did not specifically assess the effects of vincristine on IL-18 release, contributions of cytokines other than IL-1β to vincristine-induced neuropathy cannot be excluded, although several lines of evidence, including significant reductions in both mechanical allodynia and gait

Starobova et al.
Inhibition of IL-1β release prevents VIPN

Journal of Experimental Medicine
https://doi.org/10.1084/jem.20201452

9 of 16

disturbances in $Il1b^{-/-}$ mice and $Il1r1^{-/-}$ mice and after treatment with anakinra, support a major role for IL-1β signaling. Interestingly, anakinra and vincristine are both relatively poorly blood–brain barrier permeant, suggesting that vincristine-induced neuropathy is predominantly a peripherally driven pathology, despite previous reports of vincristine-induced inflammatory changes in the spinal cord (Qin et al., 2020). This hypothesis is further supported by our observation that i.pl. administration of vincristine-treated macrophages led to symptoms of mechanical allodynia (Fig. 4). IL-1β is well known to elicit sensory neuron sensitization via post-translational modification of a range of ion channels, including transient receptor potential channels TRPA1 and TRPV1, N-methyl-D-aspartic acid, and γ-aminobutyric acid receptors, as well as voltage-gated K^+, Ca^{2+}, and Na^+ channels (Binshtok et al., 2008; Ren and Torres, 2009; Schäfers and Sorkin, 2008; Stemkowski et al., 2015). In addition, secondary production of nitric oxide, bradykinin, or prostaglandins, which also modulate neuronal excitability, further contributes to IL-1β–mediated pain (Ren and Torres, 2009; Schäfers and Sorkin, 2008). Notably, intradermal injection of IL-1β causes pain hypersensitivity that is reduced, although not entirely abrogated, in $Na_V1.9^{-/-}$ animals (Amaya et al., 2006), a phenotype that was mirrored in vincristine-treated animals. While the modest reduction in vincristine-induced allodynia in $Na_V1.9^{-/-}$ animals could be considered disappointing, this observation is perhaps consistent with that of IL-1β enhancing neuronal excitability through multiple effectors. Indeed, $Na_V1.6$ was recently shown to contribute to the functional changes of DRG neurons following vincristine treatment (Chen et al., 2020). These mechanisms might explain why a range of conventional and adjuvant analgesics targeting these neuronal signaling pathways have failed to show efficacy in vincristine-induced neuropathy, and suggest that targeting NLRP3 or IL-1β signaling may be a more promising analgesic strategy.

Involvement of NLRP3 signaling has also been reported in several other painful conditions, including gout, postsurgical pain, migraine, and cancer-induced bone pain (Chen et al., 2019; Cowie et al., 2019; He et al., 2019; Starobova et al., 2020; Yin et al., 2020); however, only a few studies have used $Nlrp3^{-/-}$ animals or the specific NLRP3 inhibitor MCC950 (Chen et al., 2019; Cowie et al., 2019; Curto-Reyes et al., 2015; Deuis et al., 2017; He et al., 2016; Khan et al., 2018), and the contribution of canonical and noncanonical NLRP3 signaling pathways to pain has not been previously assessed. In postsurgical pain, mechanical allodynia was significantly attenuated in male $Nlrp3^{-/-}$ mice, but less so in female $Nlrp3^{-/-}$ mice, in which sensory neuron–specific NLRP3 contributed to allodynia (Cowie et al., 2019). In contrast, we observed no sex-specific differences in vincristine-induced neuropathy (Starobova et al., 2019a), and both male and female $Nlrp3^{-/-}$ animals were protected equally (Fig. S5). Future studies assessing the development of vincristine-induced neuropathy in sensory neuron–specific $Nlrp3^{-/-}$ animals would be of great interest, although our observation that depletion of macrophages with liposomal clodronate prevents allodynia would suggest only a minor role for NLRP3 expressed in other cell types.

Other types of immune-mediated neuropathies, such as Guillain-Barré syndrome and chronic inflammatory demyelinating polyradiculoneuropathy, are believed to arise from activation and proliferation of autoreactive T cells and other components of the adaptive immune system that ultimately cause destruction of peripheral nerves (Kieseier et al., 2018; Xu et al., 2020). In contrast, vincristine-induced neuropathy appears to predominantly involve components of the innate immune system, in particular the NLRP3 inflammasome. While our findings with the NLRP3 inhibitor MCC950 show promise for the development of vincristine-induced neuropathy, NLRP3 inhibitors are not currently approved for clinical use. In contrast, IL-1β–targeting biologics have been used extensively in both adult and pediatric populations and may thus represent an attractive, immediately available alternative, although enhanced infection risk associated with these agents may be undesirable in patients undergoing chemotherapy (Rider et al., 2016). Accordingly, additional studies are needed to evaluate the comparative efficacy of different NLRP3- and IL-1β–targeting agents to inform future clinical trials. While our data also suggest that vincristine-induced gait disturbances occur via comparable mechanisms, these are more difficult to detect in quadrupedal model organisms, and the effect of NLRP3- and IL-1β–targeting agents on foot- and wrist-drop syndrome in patients remains to be determined.

A major consideration for any treatment aimed at ameliorating chemotherapy-induced adverse effects must necessarily be the effect on tumor progression and chemotherapy efficacy, particularly in the case of inflammasome-targeting treatments where emerging evidence suggests varied disease-modifying effects. For example, tumor progression and metastasis of melanoma, gastric, and colon cancer were shown to be driven by IL-1β (Krelin et al., 2007; Li et al., 2012) and, thus, inhibition of IL1β signaling might be beneficial. On the other hand, IL-1β was also shown to contribute to the regression of murine B16 melanoma hepatic metastases (Vidal-Vanaclocha et al., 1994). In the context of the most common oncology indications for vincristine treatment, such as medulloblastomas, the role of NLRP3 and IL-1β signaling is less clear. Our results show for the first time that anakinra has, at a minimum, no clear detrimental effects on patient-derived medulloblastoma growth or vincristine-mediated tumor regression. Our studies thus suggest that addition of anakinra to chemotherapy regimens may be a viable treatment approach for the prevention of vincristine-induced neuropathy.

Although selective NLRP3 inhibitors are not yet available clinically, several compounds are currently being developed, including peripherally restricted compounds, such as somalix, which has completed phase I studies, and inzomelid, a potent, selective, central nervous system–penetrant NLRP3 inhibitor that is currently in phase Ib trials. Although selective NLRP3 inhibitors may provide favorable side effect profiles and superior efficacy (Mangan et al., 2018; Swanson et al., 2019), the translational potential for anakinra is more immediately apparent given that this biological is already in clinical use, including in children. Ultimately, the treatment approach of coadministering anakinra alongside vincristine aims to reduce

Starobova et al.
Inhibition of IL-1β release prevents VIPN

Journal of Experimental Medicine 10 of 16
https://doi.org/10.1084/jem.20201452

suffering of patients treated with vincristine and will enable patients to carry through with chemotherapy, which, in turn, will lead to better outcomes for cancer patients who are undergoing treatment with vincristine.

Conclusion

In summary, our study is the first to define the contribution of canonical and noncanonical NLRP3 signaling pathways to vincristine-induced IL-1β release in macrophages, and shows that inhibition of NLRP3 or IL-1β signaling in vivo prevents development of vincristine-induced mechanical hypersensitivity and gait abnormalities. Moreover, we have delineated novel contributions of inflammasome pathway members, including caspase-1 and the downstream effector GSDMD, to pain-like symptoms, and suggest that based on the mechanistic insights described herein, repurposing of biologics targeting IL-1β signaling is a highly promising approach to improve the therapeutic window of vincristine.

Materials and methods

Animals and ethical approvals

All behavioral experiments were performed with 8–10-wk old adult WT (C57BL/6J) mice sourced from the Animal Resource Centre or with $Nlrp3^{-/-}$, $Ice^{-/-}$ ($Casp1^{-/-}/Casp11^{null/null}$; Kayagaki et al., 2011), $Casp11^{-/-}$, $Gsdmd^{-/-}$, $Il1r1^{-/-}$, $Il1b^{-/-}$, and $Na_V1.9^{-/-}$ mice, backcrossed to C57BL/6J mice for at least five generations, of mixed sex, noting that no significant differences in VIPN were observed between sexes as reported previously (Starobova et al., 2019a) and here (Fig. S5). Animals were housed with rodent chow and water ad libitum in groups of three to five per cage under 12-h light-dark cycles and acclimatized to experiments as described previously (Starobova et al., 2019a). All experiments were performed in accordance with the 2012 Animal Care and Protection Regulation Qld; the 2013 Australian Code of Practice for the Care and Use of Animals for Scientific Purposes, eighth edition; and the International Association for the Study of Pain Guidelines for the Use of Animals in Research. Ethical approval was obtained from the University of Queensland animal ethics committee. All behavioral assessments were performed by a blinded observer, unaware of the treatment and genotype of each mouse, with animals randomized to treatment groups. Appropriate sample sizes were determined by power calculation as a minimum of $n = 4$ based on an 80% power to detect an expected 60% difference relative to baseline readings with a 20% interindividual variability between animals and a statistical significance criterion of $P < 0.05$. All animals were monitored for weight loss, general well being, and adverse effects throughout the study and were scored for the following measures: eating (score 0: drinking and eating well; score 1: change in eating or drinking habit; score 2: inappetence; score 3: not eating/ drinking, severely dehydrated); locomotion (score 0: walking normally; score 1: limping, stiffness; score 2: swollen limbs; score 3: severely restricted mobility); behavior (score 0: normal behavior; score 1: away from littermates; score 2: aggressive or huddled in corner; score 3: severe distress); and appearance (score 0: normal; score 1: ruffled fur; score 2: animal appears

depressed, hunched, reluctant to move; score 3: animal appears severely depressed). Scores of 3 in any category or ≥10 were defined as requiring immediate euthanasia. No animals showed ill health effects due to vincristine or drug treatment and genotype, with all experimental animals scoring 0 across all measures and no more than 1 for locomotion (data not shown). Weight gain was also indistinguishable from healthy animals (Fig. S1). All behavioral experiments were conducted in cohorts with WT or vehicle controls assessed at the same time, and only cohort-specific control animals were used for statistical analysis of each treatment or genotype. Therefore, controls for $Nlrp3^{-/-}$ and $Ice^{-/-}$ animals mechanical allodynia are shown in Fig. 3 A and Fig. 5 A, controls for $Casp11^{-/-}$ mechanical allodynia are shown in Fig. 5 B, controls for $Gsdmd^{-/-}$ mechanical allodynia are shown in Fig. 5 C, and controls for $Il1r1^{-/-}$, $Il1b^{-/-}$, and $Na_V1.9^{-/-}$ mechanical allodynia are shown in Fig. 5, D–F. Controls for $Nlrp3^{-/-}$ and $Ice^{-/-}$ animals gait are shown in Fig. 3 B and Fig. 6 A, controls for $Casp11^{-/-}$ and $Gsdmd^{-/-}$ gait are shown in Fig. 6, B and C, and controls for $Il1r1^{-/-}$, $Il1b^{-/-}$, and $Na_V1.9^{-/-}$ gait are shown in Fig. 6, D–F.

Drug administration for neuropathy studies

Vincristine sulfate (Sapphire Bioscience) was dissolved in sterile Dulbecco's PBS for i.p. (0.5 mg/kg) injection or in sterile-filtrated 5% glucose solution for i.pl. (10 µg; cumulative dose: 60 µg) injection. In vivo doses of vincristine were based on previous studies using well-validated murine models of vincristine-induced neuropathy (Montague et al., 2018; Old et al., 2014; Starobova et al., 2019a). Based on established conversion between murine and human doses based on body surface area, a dose of 0.5 mg/kg i.p. would be equivalent to ~1.4 mg/m², which is close to human doses ranging from 0.5 to 2.0 mg/m², particularly considering that $t_{1/2}$ is typically shorter in mice relative to humans (Nair and Jacob, 2016). For studies assessing tumor progression and chemotherapy efficacy, we used a vincristine dose of 0.25 mg/kg three times a week (days 1, 3, and 5, repeated weekly for 4 wk), as described below, due to weight loss of NSG mice at higher doses. For the assessment of mechanical allodynia, vincristine or vehicle (PBS) solution was administered via i.p. injection (10 µl/g) as described previously (Old et al., 2014); the injection schedule is displayed by black arrows in all figure panels. For the assessment of gait abnormalities, vincristine or vehicle (5% glucose) solution was administered via i.pl. injection (10 µg/10 µl per paw) as described previously (Starobova et al., 2019a); the injection schedule is displayed by black arrows in all figure panels. Oxaliplatin and cisplatin were administered as previously described (Starobova et al., 2019b). Briefly, oxaliplatin and cisplatin were dissolved in sterile-filtrated 5% glucose solution and administered by i.pl. injection at a dose of 40 µg/mouse. Behavioral assessments were conducted 24 h after administration of oxaliplatin and cisplatin, as described below. The microtubule-targeting epothilone chemotherapeutic ixabepilone was administered by i.p. injection (4 mg/kg) twice weekly for up to 8 wk. Behavioral assessments were conducted on day 35.

Drug treatment

Anakinra (Kineret; Sobi) or MCC950 (Coll et al., 2019) were diluted in PBS. Anakinra is a recombinant modified human IL1R

Starobova et al.
Inhibition of IL-1β release prevents VIPN

Journal of Experimental Medicine   11 of 16
https://doi.org/10.1084/jem.20201452

antagonist protein with relatively small molecular weight (17 kD) and a short (4–6 h) half-life that is administered by once or twice daily s.c. injection in patients (Akash et al., 2013; Calabrese, 2002). We based our doses of anakinra on previously published administration in mouse models (Abbate et al., 2008; Baamonde et al., 2007; Vallejo et al., 2014). Anakinra (100 mg/kg), MCC950 (20 mg/kg), or PBS was administered by i.p. injection once daily, together with vincristine (i.p. 0.5 mg/kg, or i.pl. 10 µg) injection, as indicated by colored arrows in corresponding figures. To validate the ability of anakinra to inhibit IL-1β signaling in vivo, recombinant mouse IL-1β (2 ng in PBS; R&D Systems) was administered in a volume of 10 µl into the right hind paw 24 h after treatment with vehicle (control; PBS; 10 µl/g i.p.) or anakinra (100 mg/kg i.p.).

Single-fiber experiments from skin-saphenous nerves
To assess the integrity of nerve terminals after vincristine treatment, we used the skin-saphenous nerve preparation to assess excitability of peripheral afferents (Israel et al., 2019). The glabrous hind paw skins of vincristine- and vehicle-treated animals was dissected with the saphenous nerve attached, placed in a recording chamber, secured hairy side down with petroleum jelly and continuously perfused with carbogenated synthetic interstitial fluid composed of (in mM): 107.8 NaCl, 3.5 KCl, 0.69 MgSO$_4$·2H$_2$O, 26.2 NaHCO$_3$, 1.67 NaH$_2$PO$_4$·2H$_2$O, 9.64 gluconic acid, 5.55 glucose, 7.6 sucrose, and 1.53 CaCl$_2$·2H$_2$O, pH 7.3. The second skin of the animal was kept at 4°C until ready for experimentation (up to 6 h postdissection). The saphenous nerve bundle of the skin was placed on a mirror in a separate recording chamber filled with paraffin oil, desheathed, and teased to smaller filaments that were placed on a platinum recording electrode. The corium of the skin was then manually probed with a blunt glass rod until single, mechanically sensitive receptive fields could be identified and subsequently classified by conduction velocity (C < 1 m/s; A > 1.6–12 m/s) after stimulation by bipolar Teflon-coated steel microelectrode (impedance 1\MΩ). Electrophysiological recordings were made with Dapsys software and the number of excitable C- and A-fiber neurons determined from $n = 3$ vincristine- and vincristine + anakinra–treated animals ($n = 6$ hind paw skins) and $n = 5$ untreated control animals ($n = 10$ hind paw skins).

Depletion of monocytes/macrophages and granulocytes
For depletion of granulocytes, mice were injected i.p. with 200 µg anti-Ly6G antibody or control antibody (Bio X Cell) 3 d before the first vincristine administration and then together with vincristine (i.p.; 0.5 mg/kg) injection as described previously (Daley et al., 2008; Starobova et al., 2019a). For depletion of monocytes, clodronate liposomes (10 µl/g of a 5-mg/ml solution) or control liposome-encapsulated PBS (Liposoma Research) were injected i.p. 3 d before the first vincristine administration and then together with vincristine (i.p.; 0.5 mg/kg) injection as described previously (Barclay et al., 2007; Old et al., 2014; Starobova et al., 2019a; Van Rooijen and Sanders, 1994). To confirm depletion of monocytes or granulocytes, the spleen or blood were collected after two doses of clodronate or Ly6G and/or 24 h after first vincristine (i.p.; 0.5 mg/kg) injection.

Human and murine macrophages inflammasome assays
Human monocyte-derived macrophages were prepared as described previously (Bierschenk et al., 2019). Murine BMMs were prepared as described previously (Schroder et al., 2012). Differentiated macrophages (day 6) were plated at a density of 10^6 cells/ml in RPMI 1640 (Gibco) supplemented with 10% heat-inactivated fetal calf serum, GlutaMAX (Life Technologies), and recombinant human CSF-1 (150 ng/ml; endotoxin free, produced in insect cells by the University of Queensland Protein Expression Facility). For inflammasome assays, on day 7 of cell differentiation, culture media was replaced with OptiMEM (Gibco BRL plus CSF-1) containing or not ultra-pure LPS (100 ng/ml; Escherichia coli K12 tlrl-peklps; InvivoGen) for 3 h, followed by treatment with vincristine (100 µM) for 4 h. Nigericin (5 µM; Sigma-Aldrich) was added 45 min before supernatant collection.

For in vivo experiments assessing the effects of i.pl. administration of macrophages, cells derived from wt or Nlrp3$^{-/-}$ animals were primed with LPS and treated with vincristine or nigericin as described above. Cells were then rinsed with ice-cold PBS, mechanically detached from the dish by washing with PBS through a blunt-needle syringe, centrifuged for 5 min at 300 g, rinsed with ice-cold PBS again, and resuspended to 5,000 cells/25 µl in PBS. Cells were then administered by i.pl. injection into the right hind paw of naive animals and behaviors were quantified as described below.

IL-1β ELISA
IL-1β secretion was quantified by ELISA (IL-1β Ready-SET-Go!; eBioscience), according to the manufacturer's protocol. The release of LDH was quantified using the CytoTox96 nonradioactive cytotoxicity assay (Promega) and plotted as a percentage of total cellular LDH (100% lysis control). Cell lysates and cell-free methanol/chloroform-precipitated supernatants were analyzed by Western blot using standard methods (Gross et al., 2011) with antibodies against IL-1β (AF-401-NA, 1:1,000; R&D Systems), caspase-1 (casper-1, 1:1,000; AdipoGen), GSDMD (EPR19828; Abcam), and GAPDH (polyclonal rabbit antibody, 1:5,000; BioScientific).

Flow cytometry
Cell suspensions were generated with 2% FCS in PBS and then incubated with the appropriate antibody cocktail for 40 min in the dark and on ice with agitation. The myeloid antibody cocktail was made in Fc (fragment crystallizable antibody region) block and contained anti-F4/80-Alexa Fluor 647 (clone BM8; AbD Serotec), anti-CD115-PE (clone AFS98; BioLegend), anti-Ly6G PE/Cy7 (clone 1A8; BioLegend), anti-Ly6C APC/Fire 750 (clone HK1.4; BioLegend), and anti-CD11b BV510 (M1/70; BioLegend). Cells were washed and resuspended in 100 µl 2% FCS in PBS. Specificity of staining was determined by comparison to unstained cells and appropriate isotype control cocktail. Five minutes before analysis, 5 µg/ml 7-amino actinomycin D (Life Technologies) was added to each tube to allow for the exclusion of dead cells. Cells were examined via flow cytometry on a Cytoflex flow cytometer (Beckman Coulter), and data were analyzed using FlowJo version 10 (Tree Star Data Analysis Software). Analyses were performed on live (7-amino actinomycin D

negative) cells after cell aggregate exclusion. Granulocytes were gated as $CD11b^+Ly6G^+$.

Immunohistochemistry (IHC) and histomorphometric methods

Vincristine-induced neuropathy is a peripheral neuropathy that develops in the longest axons first in a stocking or glove distribution (Starobova and Vetter, 2017). We therefore focused on examining macrophage infiltration in the most distal part of the peripheral nervous system, and assessed the sciatic nerve given that this is the longest nerve. Macrophage depletion was confirmed by IHC of spleen. IHC of spleen, sciatic nerve, DRG, and spinal cord tissues was performed on deparaffinized and rehydrated sections with unconjugated primary antibody against F4/80 (clone Cl:A3-1; rat anti-mouse; Novus Biological) or relevant isotype control antibody (normal rat IgG2b; BioLegend) as previously described (Batoon et al., 2019). Staining was imaged using either an Olympus BX50 microscope (Olympus) or VS120 slide scanner (Olympus) and analyzed using Visiopharm software.

All sections were deidentified and assessed in a blinded manner. Percent F4/80 staining area in spleen sections was quantified using an automated software-based approach to reduce or eliminate human bias. An algorithm was generated using the iterative training process within Visiopharm software to detect the distribution of diaminobenzidine chromogen (F4/80), hematoxylin (nuclei), and unstained areas which include blood vessels and extracellular matrix. A similar algorithm was applied to all spleen sections within an experiment. The number of $F4/80^+$ cells in nerve tissues was quantified by manual counting of positive cells in 1.7 ± 0.52 mm^2 of tissue. For both histology-based quantification methods described above, each data point represents the mean of analyses at three sectional depths/sample that were at least 50 μm apart.

Statistically significant differences were determined using a two-tailed unpaired t test or ordinary one-way ANOVA with Holm-Sidak's multiple comparisons test in PRISM 8 (GraphPad Software). A value of $P < 0.05$ was considered statistically significant.

Immunofluorescence microscopy of murine DRG and skin

For immunofluorescence studies, tissues from vehicle- and vincristine-treated animals were collected on day 1 (DRGs) or day 3 (skin) of treatment, fixed for 24 h (skin) or 1 h (DRG) in fresh 4% paraformaldehyde, cryoprotected overnight in 30% sucrose, followed by incubation in 50/50 30% sucrose/optimum cutting temperature compound (Tissue-Tek). Tissues were snap-frozen in optimum cutting temperature compound and cryosectioned with a Leica cryostat CM1950 (Leica Biosystems) into four to eight nonconsecutive 10-μm sections (DRGs) or 50-μm sections (skin) from $n = 4$ animals/group, as indicated, and stored at –80°C before staining. Slides were washed in physiological salt solution (PSS; composition [in mM]: 140 NaCl, 11.5 glucose, 5.9 KCl, 1.4 MgCl$_2$, 1.2 NaH$_2$PO$_4$, 5 NaHCO$_3$, 1.8 CaCl$_2$, 10 Hepes) before being blocked in blocking solution (1% BSA, PSS, and 0.2% Triton X-100; Sigma-Aldrich) for 30 min. Following three additional washes in PSS, sections were incubated with the following primary antibodies in blocking solution at the

indicated dilution in a humidified box overnight at 4°C: primary antibodies: polyclonal goat anti-mouse IL-1B (1:100; AF-401-NA; R&D Systems) and rabbit anti-PGP9.5 (1:500; Z5116; Dako). Secondary antibodies at the indicated dilutions in blocking solution were applied in darkness following three additional wash steps in PSS for 2 h at room temperature: secondary antibodies: goat anti-mouse IgG Alexa Fluor647 (1:1,000; A-21235; Thermo Fisher Scientific) and goat-anti-rabbit IgG Alexa Fluor 555 (1:1,000; Invitrogen). The samples were mounted in Fluoroshield solution containing DAPI (Sigma–Aldrich) and observed under a Fluoro 2 Upright Zeiss AxioImager (camera: Axiocam 506 camera with a CoolLED pE-4000 broad-spectrum light source; software: Zeiss Zen 2 with Tiling and EDF modules; magnification: 10× air Plan Apochromat, 20× air Plan Apochromat, and 40× oil Plan Neofluar). To quantify intraepidermal nerve fiber density, image analysis was conducted using FIJI software (ImageJ 1.53c) as previously described (Chen et al., 2020). Specifically, images—four to eight per animal—were converted to 8-bit (Image>Type>8-bit) before threshold adjustment using the Image>Adjust>Threshold function. PGP9.5-positive pixels in the epidermis (Analyze>Measure area) were then quantified by particle analysis (Analyze>Analyze Particles>Particles>Size >0.5 μm^2; Circularity 0.2–1.0) and the area of PGP9.5-positive pixels (μm^2) was expressed as a percentage of epidermis area.

Mechanical threshold measurements

Mechanical PWTs were assessed using an electronic von Frey apparatus (MouseMet; Topcat Metrology) as previously described (Deuis et al., 2014; Deuis et al., 2017; Starobova et al., 2019a). Prior to testing, animals were acclimatized (30 min) to the MouseMet test enclosures containing a bar bottom to permit access to the plantar hind paw. To determine the ipsilateral (right, for i.pl. and i.p. administration) hind PWT, a soft-tipped von Frey filament was placed on the plantar surface of the hind paw and pressure was increased linearly by rotating the handle of the device. Only tests falling within the predetermined linear parameter were included for analysis. The PWT was automatically determined by the TopCat von Frey apparatus software and recorded as the paw withdrawal force (g). The average of three measurements per mouse, at least 5 min apart, was computed as one biological replicate.

Motor performance assessment

Gross motor performance was assessed using the Parallel Rod Floor Test and analyzed using ANY-Maze software (version 4.70; Stoelting). Animals were placed in the Parallel Rod Floor Test apparatus and allowed to freely explore the enclosure. The distance traveled (m) and number of foot slips were recorded over 1 min using ANY-Maze software. The ataxia index was calculated by dividing the number of foot slips by the distance traveled (m).

Thermal threshold measurements

Thermal threshold measurements were conducted using a MouseMet thermal device (Topcat Metrology) as previously described (Deuis and Vetter, 2016). Animals were acclimatized to individual elevated enclosures with a bar bottom for 30 min.

Starobova et al.
Inhibition of IL-1β release prevents VIPN

Journal of Experimental Medicine   13 of 16
https://doi.org/10.1084/jem.20201452

The thermal probe was preheated to 37°C before applying it to the plantar surface of the ipsilateral (right, for i.pl. and i.p. administration) hind paw. Heating of the probe was initiated by rotation of the handle, with the heat rate set to 2.5°C/sec. A temperature cutoff was set at 55°C to prevent tissue damage. The temperature that elicited paw withdrawal was recorded from the TopCat Metrology, and the average of three measurements per mouse at least 5 min apart constituted one replicate.

Gait analysis
Examination of motoric disturbances was performed using the CatwalkXT (Noldus Information Technology) as described previously (Parvathy and Masocha, 2013). Mice were placed individually at one of the elevated enclosed glass walkways and allowed to walk freely to the other end, with a high-speed camera located below to record illuminated paw prints. The camera gain was set at 20.00 and the green intensity of the walkway at 0.10. Only runs of 3–12-s duration with speed variances below 80% were considered for analysis. Three successful runs were recorded for each animal at each time point. Data analysis was performed using CatwalkXT software.

Generation of s.c. xenografts
Studies were conducted using Group 3 MB PDX models (Med-211FH and Med-411FH) and an Shh MB PDX model (Med-1712FH), generated in the Olson laboratory (Seattle, WA), by implanting pediatric patient tumor tissue directly into the cerebellum of immunocompromised mice (NOD.Cg-Prkdcscid Il2rgtm1Wjl/Szj [NSG]) and propagating them exclusively via orthotopic transplantation into mice as previously described (Brabetz et al., 2018). Med-211FH, Med-411FH, and Med1712FH PDX tumor cells were harvested from intracranial tumors of symptomatic donor mice. Tumor tissue was triturated through a 21-G needle in serum-free DMEM to generate a single-cell suspension. Cells were filtered, centrifuged, and resuspended in serum-free DMEM 1:1 with Matrigel to a concentration of 20,000 cells/µl. 100 µl of the tumor cell suspension (2×10^6 cells) was injected s.c. into each flank of NSG mice.

PDX drug efficacy studies
Mice were randomly assigned to therapeutic treatment groups via rolling enrolment. Mice were enrolled when s.c. tumors measured 200–300 mm³ in size and treatment was administered for 4 wk or until maximum tumor size was reached (2,000 mm³), requiring ethical collection. Vincristine treatment was administered via a single i.p. dose of 0.25 mg/kg (on days 1, 3, and 5/wk × 4 wk). Anakinra treatment commenced when s.c. tumors reached 100 mm³ in size, allowing for a period of pretreatment before vincristine administration to maximize opportunities to observe effects on tumor progression. Anakinra was administered daily via a single i.p. dose of 100 mg/kg. Tumor volume measurements were taken biweekly and mouse weights were measured daily. Tumors were measured with calipers and tumor volume was calculated using the equation: (Length × Width²)/2.

Data and statistical analyses
Data and statistical analyses were performed using GraphPad PRISM version 7.00. Unless otherwise specified, statistical significance was determined as adjusted P value < 0.05 and was calculated using two-way ANOVA with Tukey's multiple comparisons test or with repeated measures two-way ANOVA with Sidak's multiple comparisons test for behavioral data. All data are shown as mean ± SEM; $n \geq 6$ for all groups (three or more females and three males), and all experimental groups were compared with vehicle group (control) or baseline as indicated.

Online supplemental material
Fig. S1 describes the effect of vincristine on weight gain, motor performance, or heat sensitivity in C57BL6 mice. Fig. S2 describes the effect of vincristine and nigericin on the NLRP3 inflammasome in BMMs and effects of anakinra on IL-1β–induced allodynia. Fig. S3 describes the effects of vincristine on peripheral nerve excitability, intraepidermal nerve fiber density, and IL-1β immunofluorescence in DRG. Fig. S4 describes the activation of the NLRP3 inflammasome in macrophages from NSG mice. Fig. S5 describes vincristine-induced neuropathy in male and female C57BL/6 and $Nlrp3^{-/-}$ mice. Table S1 lists individual values of measurements of mechanical PWT and gait disturbances for each time point of systemic or local administration of vincristine. Table S2 lists individual values of measurements of mechanical PWT for each time point of $Nlrp3^{-/-}$ or animals cotreated with MCC950 following systemic or local administration of vincristine. Table S3 lists individual values of measurements of gait disturbances for each time point of $Nlrp3^{-/-}$ or animals cotreated with MCC950 following local administration of vincristine. Table S4 lists individual values of measurements of mechanical PWT for each time point of $Ice^{-/-}$, $Gsdmd^{-/-}$, and $Casp11^{-/-}$ animals following systemic administration of vincristine. Table S5 lists individual values of measurements of mechanical PWT for each time point of $Ice^{-/-}$, $Gsdmd^{-/-}$, and $Casp11^{-/-}$ animals following local administration of vincristine. Table S6 lists individual values of measurements of mechanical PWT for each time point of $Il1b^{-/-}$, $Il1r1^{-/-}$, and $Na_V1.9^{-/-}$ animals following systemic administration of vincristine. Table S7 lists individual values of measurements of mechanical PWT for each time point of $Il1b^{-/-}$, $Il1r1^{-/-}$, and $Na_V1.9^{-/-}$ animals following local administration of vincristine. Table S8 lists individual values of measurements of gait disturbances for each time point of $Ice^{-/-}$, $Gsdmd^{-/-}$, and $Casp11^{-/-}$ animals following local administration of vincristine. Table S9 lists individual values of measurements of gait disturbances for each time point of $Il1b^{-/-}$, $Il1r1^{-/-}$, and $Na_V1.9^{-/-}$ animals following local administration of vincristine. Table S10 lists individual values of measurements of mechanical PWT and gait disturbances for each time point of C57BL6 mice cotreated with anakinra and systemic or local administration of vincristine.

References

Abbate, A., F.N. Salloum, E. Vecile, A. Das, N.N. Hoke, S. Straino, G.G. Biondi-Zoccai, J.E. Houser, I.Z. Qureshi, E.D. Ownby, et al. 2008. Anakinra, a recombinant human interleukin-1 receptor antagonist, inhibits apoptosis in experimental acute myocardial infarction. *Circulation.* 117: 2670–2683. https://doi.org/10.1161/CIRCULATIONAHA.107.740233

Akash, M.S., K. Rehman, and S. Chen. 2013. IL-1Ra and its delivery strategies: inserting the association in perspective. *Pharm. Res.* 30:2951–2966. https://doi.org/10.1007/s11095-013-1118-0

Amaya, F., H. Wang, M. Costigan, A.J. Allchorne, J.P. Hatcher, J. Egerton, T. Stean, V. Morisset, D. Grose, M.J. Gunthorpe, et al. 2006. The voltage-gated sodium channel Na(v)1.9 is an effector of peripheral inflammatory pain hypersensitivity. *J. Neurosci.* 26:12852–12860. https://doi.org/10.1523/JNEUROSCI.4015-06.2006

Baamonde, A., V. Curto-Reyes, L. Juárez, A. Meana, A. Hidalgo, and L. Menéndez. 2007. Antihyperalgesic effects induced by the IL-1 receptor antagonist anakinra and increased IL-1beta levels in inflamed and osteosarcoma-bearing mice. *Life Sci.* 81:673–682. https://doi.org/10.1016/j.lfs.2007.07.003

Barclay, J., A.K. Clark, P. Ganju, C. Gentry, S. Patel, G. Wotherspoon, F. Buxton, C. Song, J. Ullah, J. Winter, et al. 2007. Role of the cysteine protease cathepsin S in neuropathic hyperalgesia. *Pain.* 130:225–234. https://doi.org/10.1016/j.pain.2006.11.017

Batoon, L., S.M. Millard, M.E. Wullschleger, C. Preda, A.C. Wu, S. Kaur, H.W. Tseng, D.A. Hume, J.P. Levesque, L.J. Raggatt, and A.R. Pettit. 2019. CD169⁺ macrophages are critical for osteoblast maintenance and promote intramembranous and endochondral ossification during bone repair. *Biomaterials.* 196:51–66. https://doi.org/10.1016/j.biomaterials.2017.10.033

Bierschenk, D., M. Monteleone, F. Moghaddas, P.J. Baker, S.L. Masters, D. Boucher, and K. Schroder. 2019. The Salmonella pathogenicity island-2 subverts human NLRP3 and NLRC4 inflammasome responses. *J. Leukoc. Biol.* 105:401–410. https://doi.org/10.1002/JLB.MA0318-112RR

Binshtok, A.M., H. Wang, K. Zimmermann, F. Amaya, D. Vardeh, L. Shi, G.J. Brenner, R.R. Ji, B.P. Bean, C.J. Woolf, and T.A. Samad. 2008. Nociceptors are interleukin-1beta sensors. *J. Neurosci.* 28:14062–14073. https://doi.org/10.1523/JNEUROSCI.3795-08.2008

Brabetz, S., S.E.S. Leary, S.N. Gröbner, M.W. Nakamoto, H. Şeker-Cin, E.J. Girard, B. Cole, A.D. Strand, K.L. Bloom, V. Hovestadt, et al. 2018. A biobank of patient-derived pediatric brain tumor models. *Nat. Med.* 24: 1752–1761. https://doi.org/10.1038/s41591-018-0207-3

Calabrese, L.H. 2002. Anakinra treatment of patients with rheumatoid arthritis. *Ann. Pharmacother.* 36:1204–1209. https://doi.org/10.1345/aph.1A396

Chan, A.H., and K. Schroder. 2020. Inflammasome signaling and regulation of interleukin-1 family cytokines. *J. Exp. Med.* 217:e20190314. https://doi.org/10.1084/jem.20190314

Chen, S.P., Y.Q. Zhou, X.M. Wang, J. Sun, F. Cao, S. HaiSam, D.W. Ye, and Y.K. Tian. 2019. Pharmacological inhibition of the NLRP3 inflammasome as a potential target for cancer-induced bone pain. *Pharmacol. Res.* 147: 104339. https://doi.org/10.1016/j.phrs.2019.104339

Chen, L., J. Huang, C. Benson, K.L. Lankford, P. Zhao, J. Carrara, A.M. Tan, J.D. Kocsis, S.G. Waxman, and S.D. Dib-Hajj. 2020. Sodium channel Nav1.6 in sensory neurons contributes to vincristine-induced allodynia. *Brain.* 143:2421–2436. https://doi.org/10.1093/brain/awaa208

Coll, R.C., J.R. Hill, C.J. Day, A. Zamoshnikova, D. Boucher, N.L. Massey, J.L. Chitty, J.A. Fraser, M.P. Jennings, A.A.B. Robertson, and K. Schroder. 2019. MCC950 directly targets the NLRP3 ATP-hydrolysis motif for inflammasome inhibition. *Nat. Chem. Biol.* 15:556–559. https://doi.org/10.1038/s41589-019-0277-7

Cowie, A.M., A.D. Menzel, C. O'Hara, M.W. Lawlor, and C.L. Stucky. 2019. NOD-like receptor protein 3 inflammasome drives postoperative mechanical pain in a sex-dependent manner. *Pain.* 160:1794–1816. https://doi.org/10.1097/j.pain.0000000000001555

Curto-Reyes, V., G. Kirschmann, M. Pertin, S.K. Drexler, I. Decosterd, and M.R. Suter. 2015. Neuropathic Pain Phenotype Does Not Involve the NLRP3 Inflammasome and Its End Product Interleukin-1β in the Mice Spared Nerve Injury Model. *PLoS One.* 10:e0133707. https://doi.org/10.1371/journal.pone.0133707

Daley, J.M., A.A. Thomay, M.D. Connolly, J.S. Reichner, and J.E. Albina. 2008. Use of Ly6G-specific monoclonal antibody to deplete neutrophils in mice. *J. Leukoc. Biol.* 83:64–70. https://doi.org/10.1189/jlb.0407247

Deuis, J.R., and I. Vetter. 2016. The thermal probe test: A novel behavioral assay to quantify thermal paw withdrawal thresholds in mice. *Temperature.* 3:199–207. https://doi.org/10.1080/23328940.2016.1157668

Deuis, J.R., Y.L. Lim, S. Rodrigues de Sousa, R.J. Lewis, P.F. Alewood, P.J. Cabot, and I. Vetter. 2014. Analgesic effects of clinically used compounds in novel mouse models of polyneuropathy induced by oxaliplatin and cisplatin. *Neuro-oncol.* 16:1324–1332. https://doi.org/10.1093/neuonc/nou048

Deuis, J.R., K. Yin, M.A. Cooper, K. Schroder, and I. Vetter. 2017. Role of the NLRP3 inflammasome in a model of acute burn-induced pain. *Burns.* 43: 304–309. https://doi.org/10.1016/j.burns.2016.09.001

Evavold, C.L., J. Ruan, Y. Tan, S. Xia, H. Wu, and J.C. Kagan. 2018. The Pore-Forming Protein Gasdermin D Regulates Interleukin-1 Secretion from Living Macrophages. *Immunity.* 48:35–44.e6. https://doi.org/10.1016/j.immuni.2017.11.013

Gross, H., S. Barth, T. Pfuhl, V. Willnecker, A. Spurk, V. Gurtsevitch, M. Sauter, B. Hu, E. Noessner, N. Mueller-Lantzsch, et al. 2011. The NP9 protein encoded by the human endogenous retrovirus HERV-K(HML-2) negatively regulates gene activation of the Epstein-Barr virus nuclear antigen 2 (EBNA2). *Int. J. Cancer.* 129:1105–1115. https://doi.org/10.1002/ijc.25760

He, Y., H. Hara, and G. Núñez. 2016. Mechanism and Regulation of NLRP3 Inflammasome Activation. *Trends Biochem. Sci.* 41:1012–1021. https://doi.org/10.1016/j.tibs.2016.09.002

He, W., T. Long, Q. Pan, S. Zhang, Y. Zhang, D. Zhang, G. Qin, L. Chen, and J. Zhou. 2019. Microglial NLRP3 inflammasome activation mediates IL-1β release and contributes to central sensitization in a recurrent nitroglycerin-induced migraine model. *J. Neuroinflammation.* 16:78. https://doi.org/10.1186/s12974-019-1459-7

Israel, M.R., B.S. Tanaka, J. Castro, P. Thongyoo, S.D. Robinson, P. Zhao, J.R. Deuis, D.J. Craik, T. Durek, S.M. Brierley, et al. 2019. Na$_V$ 1.6 regulates excitability of mechanosensitive sensory neurons. *J. Physiol.* 597: 3751–3768. https://doi.org/10.1113/JP278148

Kautio, A.L., M. Haanpää, H. Kautiainen, E. Kalso, and T. Saarto. 2011. Burden of chemotherapy-induced neuropathy--a cross-sectional study. *Support. Care Cancer.* 19:1991–1996. https://doi.org/10.1007/s00520-010-1043-2

Kayagaki, N., S. Warming, M. Lamkanfi, L. Vande Walle, S. Louie, J. Dong, K. Newton, Y. Qu, J. Liu, S. Heldens, et al. 2011. Non-canonical inflammasome activation targets caspase-11. *Nature.* 479:117–121. https://doi.org/10.1038/nature10558

Kelley, N., D. Jeltema, Y. Duan, and Y. He. 2019. The NLRP3 Inflammasome: An Overview of Mechanisms of Activation and Regulation. *Int. J. Mol. Sci.* 20:3328. https://doi.org/10.3390/ijms20133328

Khan, N., A. Kuo, D.A. Brockman, M.A. Cooper, and M.T. Smith. 2018. Pharmacological inhibition of the NLRP3 inflammasome as a potential target for multiple sclerosis induced central neuropathic pain. *Inflammopharmacology.* 26:77–86. https://doi.org/10.1007/s10787-017-0401-9

Kieseier, B.C., E.K. Mathey, C. Sommer, and H.P. Hartung. 2018. Immune-mediated neuropathies. *Nat. Rev. Dis. Primers.* 4:31. https://doi.org/10.1038/s41572-018-0027-2

Kiguchi, N., T. Maeda, Y. Kobayashi, F. Saika, and S. Kishioka. 2009. Involvement of inflammatory mediators in neuropathic pain caused by vincristine. *Int. Rev. Neurobiol.* 85:179–190. https://doi.org/10.1016/S0074-7742(09)85014-9

Krelin, Y., E. Voronov, S. Dotan, M. Elkabets, E. Reich, M. Fogel, M. Huszar, Y. Iwakura, S. Segal, C.A. Dinarello, and R.N. Apte. 2007. Interleukin-1beta-driven inflammation promotes the development and invasiveness of chemical carcinogen-induced tumors. *Cancer Res.* 67:1062–1071. https://doi.org/10.1158/0008-5472.CAN-06-2956

Kuyrukluyıldız, U., İ. Küpeli, Z. Bedir, Ö. Özmen, D. Onk, B. Süleyman, R. Mammadov, and H. Süleyman. 2016. The Effect of Anakinra on Paclitaxel-Induced Peripheral Neuropathic Pain in Rats. *Turk. J. Anaesthesiol. Reanim.* 44:287–294. https://doi.org/10.5152/TJAR.2016.02212

LaPointe, N.E., G. Morfini, S.T. Brady, S.C. Feinstein, L. Wilson, and M.A. Jordan. 2013. Effects of eribulin, vincristine, paclitaxel and ixabepilone on fast axonal transport and kinesin-1 driven microtubule gliding: implications for chemotherapy-induced peripheral neuropathy. *Neurotoxicology.* 37:231–239. https://doi.org/10.1016/j.neuro.2013.05.008

Li, Y., L. Wang, L. Pappan, A. Galliher-Beckley, and J. Shi. 2012. IL-1β promotes stemness and invasiveness of colon cancer cells through Zeb1 activation. *Mol. Cancer.* 11:87. https://doi.org/10.1186/1476-4598-11-87

Lu, F., Z. Lan, Z. Xin, C. He, Z. Guo, X. Xia, and T. Hu. 2020. Emerging insights into molecular mechanisms underlying pyroptosis and functions of inflammasomes in diseases. *J. Cell. Physiol.* 235:3207–3221. https://doi.org/10.1002/jcp.29268

Mangan, M.S.J., E.J. Olhava, W.R. Roush, H.M. Seidel, G.D. Glick, and E. Latz. 2018. Targeting the NLRP3 inflammasome in inflammatory diseases. *Nat. Rev. Drug Discov.* 17:588–606. https://doi.org/10.1038/nrd.2018.97

Montague, K., R. Simeoli, J. Valente, and M. Malcangio. 2018. A novel interaction between CX_3CR_1 and CCR_2 signalling in monocytes constitutes an underlying mechanism for persistent vincristine-induced pain. *J. Neuroinflammation.* 15:101. https://doi.org/10.1186/s12974-018-1116-6

Mora, E., E.M. Smith, C. Donohoe, and D.L. Hertz. 2016. Vincristine-induced peripheral neuropathy in pediatric cancer patients. *Am. J. Cancer Res.* 6:2416–2430.

Mulvihill, E., L. Sborgi, S.A. Mari, M. Pfreundschuh, S. Hiller, and D.J. Müller. 2018. Mechanism of membrane pore formation by human gasdermin-D. *EMBO J.* 37:e98321. https://doi.org/10.15252/embj.201798321

Nair, A.B., and S. Jacob. 2016. A simple practice guide for dose conversion between animals and human. *J. Basic Clin. Pharm.* 7:27–31. https://doi.org/10.4103/0976-0105.177703

Nama, N., M.K. Barker, C. Kwan, C. Sabarre, V. Solimano, A. Rankin, J. Raabe, C.J. Ross, B. Carleton, J.G. Zwicker, and S.R. Rassekh. 2020. Vincristine-induced peripheral neurotoxicity: A prospective cohort. *Pediatr. Hematol. Oncol.* 37:15–28. https://doi.org/10.1080/08880018.2019.1677832

Old, E.A., S. Nadkarni, J. Grist, C. Gentry, S. Bevan, K.W. Kim, A.J. Mogg, M. Perretti, and M. Malcangio. 2014. Monocytes expressing CX3CR1 orchestrate the development of vincristine-induced pain. *J. Clin. Invest.* 124:2023–2036. https://doi.org/10.1172/JCI71389

Parvathy, S.S., and W. Masocha. 2013. Gait analysis of C57BL/6 mice with complete Freund's adjuvant-induced arthritis using the CatWalk system. *BMC Musculoskelet. Disord.* 14:14. https://doi.org/10.1186/1471-2474-14-14

Pilat, D., A. Piotrowska, E. Rojewska, A. Jurga, J. Ślusarczyk, W. Makuch, A. Basta-Kaim, B. Przewlocka, and J. Mika. 2016. Blockade of IL-18 signaling diminished neuropathic pain and enhanced the efficacy of morphine and buprenorphine. *Mol. Cell. Neurosci.* 71:114–124. https://doi.org/10.1016/j.mcn.2015.12.013

Qin, B., Y. Li, X. Liu, D. Gong, and W. Zheng. 2020. Notch activation enhances microglial CX3CR1/P38 MAPK pathway in rats model of vincristine-induced peripheral neuropathy. *Neurosci. Lett.* 715:134624. https://doi.org/10.1016/j.neulet.2019.134624

Ren, K., and R. Torres. 2009. Role of interleukin-1beta during pain and inflammation. *Brain Res. Brain Res. Rev.* 60:57–64. https://doi.org/10.1016/j.brainresrev.2008.12.020

Rider, P., Y. Carmi, and I. Cohen. 2016. Biologics for Targeting Inflammatory Cytokines, Clinical Uses, and Limitations. *Int. J. Cell Biol.* 2016:9259646. https://doi.org/10.1155/2016/9259646

Schäfers, M., and L. Sorkin. 2008. Effect of cytokines on neuronal excitability. *Neurosci. Lett.* 437:188–193. https://doi.org/10.1016/j.neulet.2008.03.052

Schroder, K., K.M. Irvine, M.S. Taylor, N.J. Bokil, K.A. Le Cao, K.A. Masterman, L.I. Labzin, C.A. Semple, R. Kapetanovic, L. Fairbairn, et al. 2012. Conservation and divergence in Toll-like receptor 4-regulated gene expression in primary human versus mouse macrophages. *Proc. Natl. Acad. Sci. USA.* 109:E944–E953. https://doi.org/10.1073/pnas.1110156109

Son, S., D.W. Shim, I. Hwang, J.H. Park, and J.W. Yu. 2019. Chemotherapeutic Agent Paclitaxel Mediates Priming of NLRP3 Inflammasome Activation. *Front. Immunol.* 10:1108. https://doi.org/10.3389/fimmu.2019.01108

Starobova, H., and I. Vetter. 2017. Pathophysiology of Chemotherapy-Induced Peripheral Neuropathy. *Front. Mol. Neurosci.* 10:174. https://doi.org/10.3389/fnmol.2017.00174

Starobova, H., A. Mueller, R. Allavena, R.J. Lohman, M.J. Sweet, and I. Vetter. 2019a. Minocycline Prevents the Development of Mechanical Allodynia in Mouse Models of Vincristine-Induced Peripheral Neuropathy. *Front. Neurosci.* 13:653. https://doi.org/10.3389/fnins.2019.00653

Starobova, H., A. Mueller, J.R. Deuis, D.A. Carter, and I. Vetter. 2019b. Inflammatory and Neuropathic Gene Expression Signatures of Chemotherapy-Induced Neuropathy Induced by Vincristine, Cisplatin, and Oxaliplatin in C57BL/6J Mice. *J. Pain.* 21:182–194. https://doi.org/10.1016/j.jpain.2019.06.008

Starobova, H., E.I. Nadar, and I. Vetter. 2020. The NLRP3 Inflammasome: Role and Therapeutic Potential in Pain Treatment. *Front. Physiol.* 11:1016. https://doi.org/10.3389/fphys.2020.01016

Stemkowski, P.L., M.C. Noh, Y. Chen, and P.A. Smith. 2015. Increased excitability of medium-sized dorsal root ganglion neurons by prolonged interleukin-1β exposure is K(+) channel dependent and reversible. *J. Physiol.* 593:3739–3755. https://doi.org/10.1113/JP270905

Swanson, K.V., M. Deng, and J.P. Ting. 2019. The NLRP3 inflammasome: molecular activation and regulation to therapeutics. *Nat. Rev. Immunol.* 19:477–489. https://doi.org/10.1038/s41577-019-0165-0

Uçeyler, N., I. Kobsar, L. Biko, J. Ulzheimer, S.R. Levinson, R. Martini, and C. Sommer. 2006. Heterozygous P0 deficiency protects mice from vincristine-induced polyneuropathy. *J. Neurosci. Res.* 84:37–46. https://doi.org/10.1002/jnr.20873

Vallejo, S., E. Palacios, T. Romacho, L. Villalobos, C. Peiró, and C.F. Sánchez-Ferrer. 2014. The interleukin-1 receptor antagonist anakinra improves endothelial dysfunction in streptozotocin-induced diabetic rats. *Cardiovasc. Diabetol.* 13:158. https://doi.org/10.1186/s12933-014-0158-z

Van Rooijen, N., and A. Sanders. 1994. Liposome mediated depletion of macrophages: mechanism of action, preparation of liposomes and applications. *J. Immunol. Methods.* 174:83–93. https://doi.org/10.1016/0022-1759(94)90012-4

Vidal-Vanaclocha, F., C. Amézaga, A. Asumendi, G. Kaplanski, and C.A. Dinarello. 1994. Interleukin-1 receptor blockade reduces the number and size of murine B16 melanoma hepatic metastases. *Cancer Res.* 54:2667–2672.

Wang, M.S., Y. Wu, D.G. Culver, and J.D. Glass. 2000. Pathogenesis of axonal degeneration: parallels between Wallerian degeneration and vincristine neuropathy. *J. Neuropathol. Exp. Neurol.* 59:599–606. https://doi.org/10.1093/jnen/59.7.599

Weintraub, M., M.A. Adde, D.J. Venzon, A.T. Shad, I.D. Horak, J.E. Neely, N.L. Seibel, J. Gootenberg, C. Arndt, M.L. Nieder, and I.T. Magrath. 1996. Severe atypical neuropathy associated with administration of hematopoietic colony-stimulating factors and vincristine. *J. Clin. Oncol.* 14:935–940. https://doi.org/10.1200/JCO.1996.14.3.935

Xu, M., D.L.H. Bennett, L.A. Querol, L.J. Wu, S.R. Irani, J.C. Watson, S.J. Pittock, and C.J. Klein. 2020. Pain and the immune system: emerging concepts of IgG-mediated autoimmune pain and immunotherapies. *J. Neurol. Neurosurg. Psychiatry.* 91:177–188. https://doi.org/10.1136/jnnp-2018-318556

Yin, C., B. Liu, P. Wang, X. Li, Y. Li, X. Zheng, Y. Tai, C. Wang, and B. Liu. 2020. Eucalyptol alleviates inflammation and pain responses in a mouse model of gout arthritis. *Br. J. Pharmacol.* 177:2042–2057. https://doi.org/10.1111/bph.14967

Yu, X., H. Liu, K.A. Hamel, M.G. Morvan, S. Yu, J. Leff, Z. Guan, J.M. Braz, and A.I. Basbaum. 2020. Dorsal root ganglion macrophages contribute to both the initiation and persistence of neuropathic pain. *Nat. Commun.* 11:264. https://doi.org/10.1038/s41467-019-13839-2
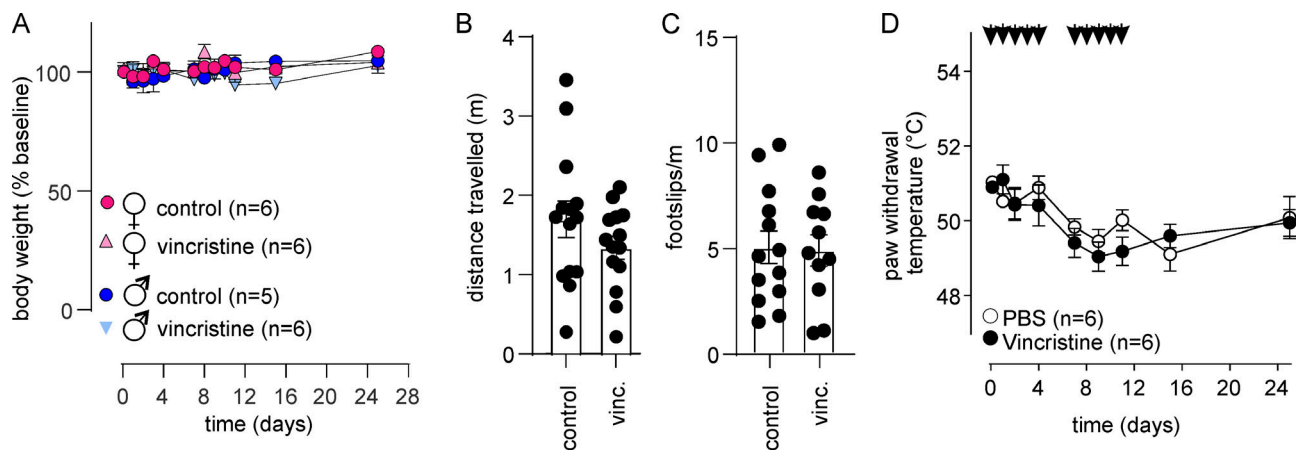
Supplemental material

Figure S1. **Effect of vincristine on weight gain, motor performance, and heat sensitivity in C57BL/6 mice. (A–C)** Vincristine (0.5 mg/kg i.p.) does not affect weight gain (P > 0.05 by two-way repeated measures ANOVA) in either males or females (A), and does not affect motor performance (B and C), assessed using the parallel rod floor apparatus. Both distance traveled (m; B) and foot slips/m (C) were unchanged (P > 0.05 by unpaired t test) in vincristine-treated animals compared with control. **(D)** Vincristine (0.5 mg/kg i.p.) does not cause heat allodynia, with PWTs unchanged compared with PBS-treated animals (P > 0.05 by two-way repeated measures ANOVA). All data are shown as mean ± SEM; n ≥5 for all groups as indicated.
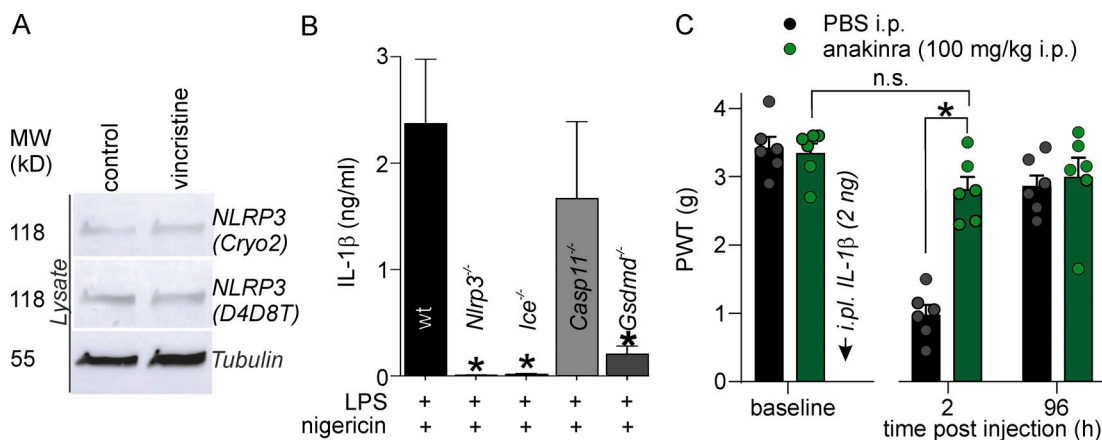

Figure S2. **Effect of vincristine and nigericin on the NLRP3 inflammasome in BMMs, and effects of anakinra on IL-1β-induced allodynia. (A)** Vincristine treatment does not increase NLRP3 expression in macrophages, assessed by Western blotting using two anti-NLRP3 antibodies (Cryo2 and D4D8T). MW, molecular weight. **(B)** Nigericin-induced IL-1β release in LPS-primed C57BL6/J, $Nlrp3^{-/-}$, $Ice^{-/-}$, $Casp11^{-/-}$, and $Gsdmd^{-/-}$ BMMs. Incubation time of Nigericin: 45 min. Statistical significance was determined using ordinary one-way ANOVA with multiple comparison. n = 3 independent experiments for all groups. **(C)** Decreased PWT induced by i.pl. injection of IL-1β (black bars) is prevented by treatment with anakinra (100 mg/kg i.p., green bars). n = 6 animals/group. Statistical significance was determined using ordinary two-way ANOVA with multiple comparison. All data are shown as mean ± SEM; *, P < 0.05. MW, molecular weight.
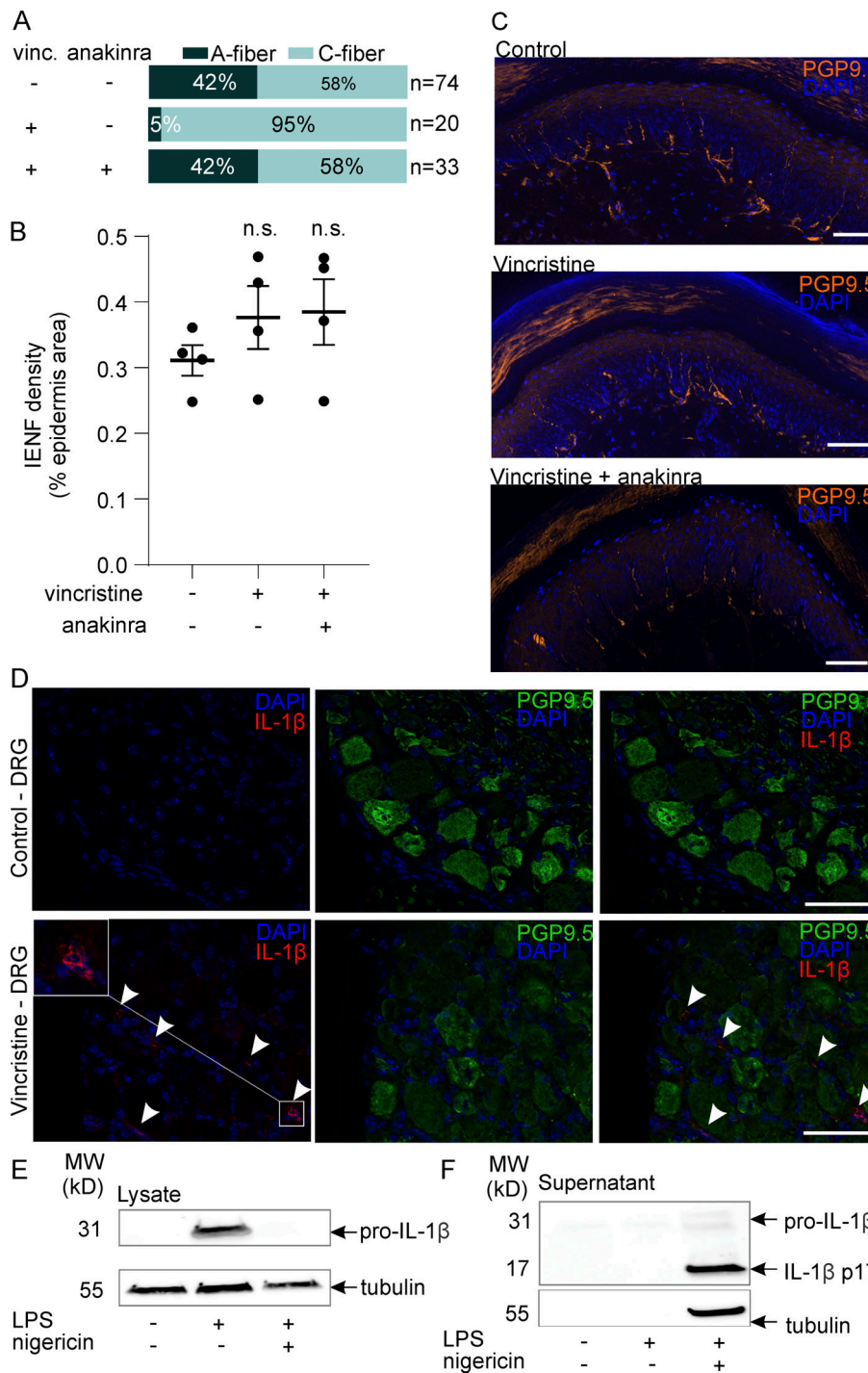
Figure S3. **Effects of vincristine on peripheral nerve excitability, intraepidermal nerve fiber density, and IL-1β immunofluorescence in dorsal root ganglia. (A)** The proportion of excitable myelinated A-fibers is reduced from 31/74 fibers in control animals (recordings from *n* = 5 animals) to 1/20 fibers after treatment with vincristine (vinc; recordings from *n* = 3 animals), and rescued (to 14/33 fibers) by anakinra (100 mg/kg i.p.; recordings from *n* = 3 animals). Excitable A- and C-fibers were classified by conduction velocity and quantified from single-fiber recordings using the murine skin-saphenous nerve preparation. **(B and C)** Vincristine treatment does not reduce the density of intraepidermal nerve fibers (IENFs; P > 0.05 by one-way ANOVA). **(B)** Area of pan-neuronal PGP9.5-positive immunofluorescence (percent epidermal area) from four to six nonconsecutive 50-μm skin sections taken from animals (*n* = 4/group) treated with PBS (control), vincristine (0.5 mg/kg i.p.), and vincristine + anakinra (0.5 mg/kg i.p./100 mg/kg i.p.) for 72 h. **(C)** Representative apotome images of IENFs in hind paw skin samples from control, vincristine-, and vincristine + anakinra-treated mice. Scale bar: 50 μm. **(D)** Representative immunofluorescence images of DRG sections (10 μm) from vehicle- and vincristine-treated mice stained with the pan-neuronal marker PGP9.5 (green) and anti–IL-1β (red; AF-401NA; R&D Systems). Arrowheads: IL-1β–positive cells are observed in close proximity to PGP9.5-positive DRG neuron cell bodies. Scale bar: 50 μm. **(E and F)** Anti–IL-1β antibody AF-401NA detects uncleaved pro–IL-1β in cell lysates from LPS-primed macrophages (E), as well as cleaved, mature IL-1β secreted into cell supernatants by LPS-primed, nigericin-treated macrophages (F). MW, molecular weight.

Starobova et al.
Inhibition of IL-1β release prevents VIPN

Journal of Experimental Medicine   S2
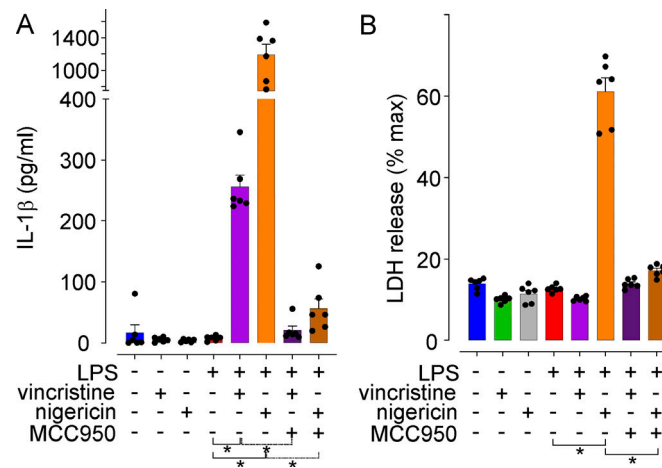https://doi.org/10.1084/jem.20201452

Figure S4. **Activation of the NLRP3 inflammasome in macrophages from NSG mice. (A)** LPS-primed, but not unprimed, macrophages isolated from NSG mice respond to both vincristine and nigericin with an increase in secreted IL-1β that is reversed by treatment with the NLRP3 inhibitor MCC950. **(B)** Nigericin treatment induced pyroptosis, evidenced by an increase in LDH release, in LPS-primed macrophages from NSG mice. All data are shown as mean ± SEM; n = 6 replicates for all groups. Statistical significance was determined by one-way ANOVA. *, P < 0.05.
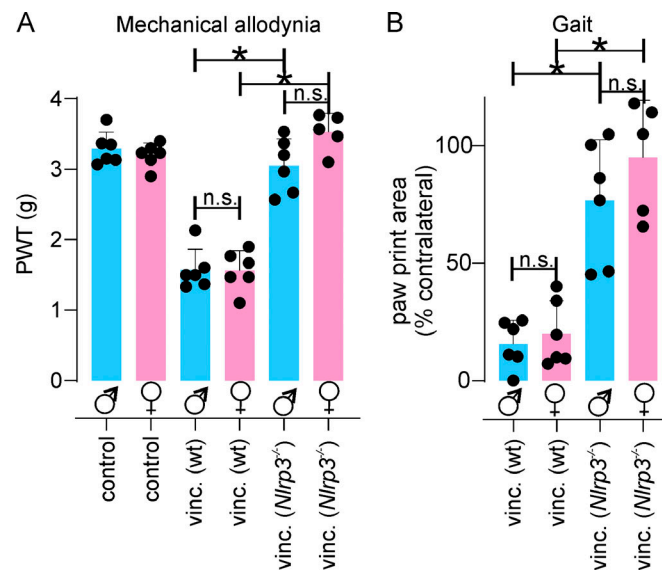

Figure S5. **Vincristine-induced neuropathy in male and female C57BL/6 and $Nlrp3^{-/-}$ mice. (A and B)** Vincristine (vinc)-induced mechanical allodynia (A) and gait disturbances (B) develop in both male (blue) and female (pink) animals. Both male and female $Nlrp3^{-/-}$ animals are protected from vincristine-induced mechanical allodynia (A) and gait disturbances (B). All data are shown as mean ± SEM; n ≥5 for all groups. Statistical significance was determined by one-way ANOVA with Sidak's post-test. *, P < 0.05.

Provided online are ten tables. Table S1 lists individual values of measurements of mechanical PWT and gait disturbances for each time point of systemic or local administration of vincristine. Table S2 lists individual values of measurements of mechanical PWT for each time point of $Nlrp3^{-/-}$ or animals cotreated with MCC950 following systemic or local administration of vincristine. Table S3 lists individual values of measurements of gait disturbances for each time point of $Nlrp3^{-/-}$ or animals cotreated with MCC950 following local administration of vincristine. Table S4 lists individual values of measurements of mechanical PWT for each time point of $Ice^{-/-}$, $Gsdmd^{-/-}$, and $Casp11^{-/-}$ animals following systemic administration of vincristine. Table S5 lists individual values of measurements of mechanical PWT for each time point of $Ice^{-/-}$, $Gsdmd^{-/-}$, and $Casp11^{-/-}$ animals following local administration of vincristine. Table S6 lists individual values of measurements of mechanical PWT for each time point of $Il1b^{-/-}$, $Il1r1^{-/-}$, and $Na_V1.9^{-/-}$ animals following systemic administration of vincristine. Table S7 lists individual values of measurements of mechanical PWT for each time point of $Il1b^{-/-}$, $Il1r1^{-/-}$, and $Na_V1.9^{-/-}$ animals following local administration of vincristine. Table S8 lists individual values of measurements of gait disturbances for each time point of $Ice^{-/-}$, $Gsdmd^{-/-}$, and $Casp11^{-/-}$ animals following local administration

of vincristine. Table S9 lists individual values of measurements of gait disturbances for each time point of *Il1b*$^{-/-}$, *Il1r1*$^{-/-}$, and *Na$_V$1.9*$^{-/-}$ animals following local administration of vincristine. Table S10 lists individual values of measurements of mechanical PWT and gait disturbances for each time point of C57BL6 mice cotreated with anakinra and systemic or local administration of vincristine.